

FIGRET: Fine-Grained Robustness-Enhanced Traffic Engineering

Ximeng Liu
Shanghai Jiao Tong University

Yong Cui
Tsinghua University

Shizhen Zhao*
Shanghai Jiao Tong University

Xinbing Wang
Shanghai Jiao Tong University

ABSTRACT

Traffic Engineering (TE) is critical for improving network performance and reliability. A key challenge in TE is the management of sudden traffic bursts. Existing TE schemes either do not handle traffic bursts or uniformly guard against traffic bursts, thereby facing difficulties in achieving a balance between normal-case performance and burst-case performance. To address this issue, we introduce FIGRET, a Fine-Grained Robustness-Enhanced TE scheme. FIGRET offers a novel approach to TE by providing varying levels of robustness enhancements, customized according to the distinct traffic characteristics of various source-destination pairs. By leveraging a burst-aware loss function and deep learning techniques, FIGRET is capable of generating high-quality TE solutions efficiently. Our evaluations of real-world production networks, including Wide Area Networks and data centers, demonstrate that FIGRET significantly outperforms existing TE schemes. Compared to the TE scheme currently deployed in Google's Jupiter data center networks, FIGRET achieves a 9%-34% reduction in average Maximum Link Utilization and improves solution speed by 35×-1800×. Against DOTE, a state-of-the-art deep learning-based TE method, FIGRET substantially lowers the occurrence of significant congestion events triggered by traffic bursts by 41%-53.9% in topologies with high traffic dynamics.

CCS CONCEPTS

• **Networks** → Traffic engineering algorithms; • **Computing methodologies** → Machine learning.

KEYWORDS

Traffic engineering, Wide-Area Networks, Datacenter networks, Machine learning

ACM Reference Format:

Ximeng Liu, Shizhen Zhao, Yong Cui, and Xinbing Wang. 2024. FIGRET: Fine-Grained Robustness-Enhanced Traffic Engineering. In *ACM SIGCOMM 2024 Conference (ACM SIGCOMM '24)*, August 4–8, 2024, Sydney, NSW, Australia. ACM, New York, NY, USA, 19 pages. <https://doi.org/10.1145/3651890.3672258>

*Shizhen Zhao is the corresponding author.

Permission to make digital or hard copies of all or part of this work for personal or classroom use is granted without fee provided that copies are not made or distributed for profit or commercial advantage and that copies bear this notice and the full citation on the first page. Copyrights for third-party components of this work must be honored. For all other uses, contact the owner/author(s).

ACM SIGCOMM '24, August 4–8, 2024, Sydney, NSW, Australia

© 2024 Copyright held by the owner/author(s).

ACM ISBN 979-8-4007-0614-1/24/08

<https://doi.org/10.1145/3651890.3672258>

1 INTRODUCTION

With the exponential growth in network traffic, both data center networks [6, 7, 11, 14, 16, 37, 44] and Wide Area Networks (WANs) [9, 19, 20, 25–27, 31, 40, 43, 49, 52, 56] are increasingly dependent on Traffic Engineering (TE) to optimize network performance. TE, typically enabled by a centralized controller in Software-Defined Networking (SDN) [3, 5, 13, 23, 24, 30, 32, 37, 54], periodically solves optimization problems to efficiently route traffic across network paths, and then translates these solutions into router configurations.

A major challenge in TE is managing sudden traffic bursts. Considering the latency introduced by the central controller in collecting traffic demands, computing new TE solutions, and updating forwarding rules, a TE system should pre-compute network configurations based on historical data prior to the arrival of actual traffic flows. Yet, the inherently dynamic and unpredictable nature of real network traffic poses significant forecasting difficulties [46, 51]. Inadequate preparation for traffic bursts may result in severe network congestion, leading to prolonged delays, high packet loss rates, and diminished network throughput [49]. Thus, enhancing the robustness against unexpected traffic bursts is essential.

Existing burst-aware TE schemes usually handle traffic bursts at the cost of compromised normal-case network performance. Oblivious routing [9] optimizes TE solutions for the worst-case scenario across all traffic demands. While this approach offers the highest level of robustness against traffic bursts, it tends to result in highly suboptimal performance for non-burst traffic patterns, which constitute the majority of traffic over time. As an improvement, Cope [49] focuses on optimizing the predicted traffic demands while providing a worst-case performance guarantee. However, offering such a worst-case guarantee may still be an overkill because some traffic patterns may never occur. In addition, the computational complexity of COPE is also much higher. Consequently, a new class of TE methods [37, 44, 45, 49] are proposed. These TE methods do not offer guarantee in the entire traffic pattern space, but instead enhance robustness by directly limiting the routing weights of different paths. Specifically, COUDER [45] introduces the *path sensitivity* metric to evaluate the impact of burst traffic on each path, and enhances robustness by minimizing the maximum sensitivity across all paths. Similarly, Google's optical data centers adopt a hedging mechanism in TE[37], which enhances robustness by confining the path sensitivity under a predetermined upper limit. However, these methods may still impact TE performance under non-burst traffic scenarios because they force traffic to spread across multiple (potentially longer) paths rather than taking the best path, even if the traffic between certain source-destination pairs is stable.

The limitations observed in the previous methods can be attributed to their uniform treatment against traffic bursts. In practice, network traffic exhibits different characteristics among different source-destination pairs. While some pairs may frequently encounter traffic bursts, others could remain remarkably stable. For consistently stable traffic, prioritizing robustness becomes unnecessary and may even hurt performance.

Building upon this observation, we design FIGRET (Fine-Grained Robustness-Enhanced Traffic Engineering). FIGRET's *key insight* lies in a fine-grained customized robustness enhancement strategy, tailored for every source-destination pair based on their traffic characteristics. It applies relaxed robustness requirements to source-destination pairs with stable traffic and enforces stricter requirements for those prone to bursts. Similar to [44], FIGRET also uses the path sensitivity metric to enhance robustness against traffic bursts. On top of this, FIGRET customizes the path sensitivity constraints according to the network topology and the traffic characteristics of different source-destination pairs. This strategy allows FIGRET to achieve fine-grained robustness enhancement and ensure a satisfactory balance in TE performance between both normal and burst traffic scenarios.

Having proposed the FIGRET formulation, the next challenge is to efficiently compute a TE solution. At first glance, FIGRET's formulation can be directly solved using linear programming. However, this method has two shortcomings. First, directly solving FIGRET requires a predicted traffic matrix. However, due to the existence of highly bursty source-destination pairs, finding an appropriate traffic prediction is difficult. Second, linear programming involves high computational complexity and may not scale to large networks. To address these issues, FIGRET leverages a deep neural network to accelerate TE computation. Similar to DOTE [36], FIGRET directly maps a history of traffic patterns to a routing weight configuration, thus eliminating the need of traffic prediction. To handle the path sensitivity constraints, FIGRET adds an additional term in its loss function to capture the customized robustness requirement.

We conduct a comprehensive evaluation of FIGRET. This evaluation utilizes publicly available WAN datasets [47], as well as Data Center PoD-level and ToR-level topologies and traffic data [8, 41]. The data encompasses topologies ranging from dozens to hundreds of nodes, with the corresponding traffic data exhibiting various characteristics, including profiles with low, moderate, and high burstiness. Through our evaluation, we find that FIGRET consistently delivers high-quality TE solutions across a variety of topologies. Compared to the TE system in Google's production data center [37], FIGRET achieves an average Max Link Utilization (MLU) reduction of 9%-34% across different topologies and improves solution speed by 35x-1800x. In comparison with the state-of-the-art Deep Learning-based TE system DOTE [36], specifically designed for MLU optimization, FIGRET achieves notable improvements in two topologies with bursty traffic data. It reduced the average Max Link MLU by 4.5% and 5.3% while simultaneously decreasing the number of significant congestion incidents caused by traffic bursts by 41% and 53.9%. Meanwhile, in topologies with stable traffic data, FIGRET performs at least as well as DOTE, despite of the additional consideration of robustness. Finally, we numerically interpret FIGRET's superior performance. Our code is available at [1].

This work does not raise any ethical concerns.

2 MOTIVATION AND KEY INSIGHTS

2.1 Necessity of managing bursts

Traffic engineering has been adopted in both Wide Area Networks (e.g., Google's B4 [24] and Microsoft's SWAN [23]) and data centers (e.g., Google's optical data center network [37]) to improve network utilization and prevent network congestion.

To motivate the need to manage bursts in TE, we present an analysis of the impact of bursts on network performance and summarize the results in Figure 1. We implement two strategies in this study: 1) the 'No hedging' strategy, which uses the current traffic matrix to determine the TE configuration for the next interval without any approach to manage bursts; 2) the 'Hedging' strategy, which uses the current traffic matrix for configuring the next interval but incorporates the anti-burst Hedging mechanism utilized by Google in their Jupiter data center network [37]. The underlying principle of the Hedging mechanism is to spread a flow across multiple paths to prevent bursts from excessively impacting any single path. We conduct evaluations on the GEANT WAN [47], and the PoD/ToR-level direct connect topologies¹ with traffic traces collected in Meta's data centers [41]. Since GEANT WAN only offers minute-level traffic matrices, for fair comparison, we also aggregate Meta's data center traffic trace at minute-level intervals. Our findings from Figure 1 include:

- Performance sensitivity to network variability: From the GEANT WAN network to the PoD-level data center network, and then to the ToR-level data center network, traffic becomes more volatile, and the performance of the 'No hedging' strategy becomes increasingly unstable.
- Necessity of burst resistance: Across WAN and data center networks at both the ToR and PoD levels, the 'No hedging' strategy results in higher peaks on the MLU curve, indicating that the networks experience congestion due to bursts if anti-burst strategies are not employed.
- Performance trade-offs with burst resistance: The 'No hedging' strategy displays higher peaks and lower troughs on the MLU curve. This can be interpreted as peaks occurring during bursts and troughs occurring in their absence. Conversely, the 'Hedging' strategy does not achieve as low troughs during non-burst conditions, because it forces a significant portion of traffic to take non-optimal paths.

In summary, managing bursts is necessary for TE, yet strategies for burst management often compromise non-burst scenario performance. So we seek a TE method that effectively manages bursts while minimizing the impact on non-burst scenario performance.

2.2 Diversity in traffic characteristics

We find that although traffic bursts occur, the extent of these bursts varies among different source-destination pairs (SD pairs). To demonstrate the diverse traffic characteristics under different SD pairs, we provide an analysis of traffic characteristics across SD pairs in various production networks. This includes the WAN network GEANT [47], as well as the Meta's data center network

¹We change the topology from clos topologies to direct-connect topologies, because TE is rarely used in clos topologies. As optical circuit switching witnessed widespread adoption in Google's data centers [37], direct-connect topologies have become popular.

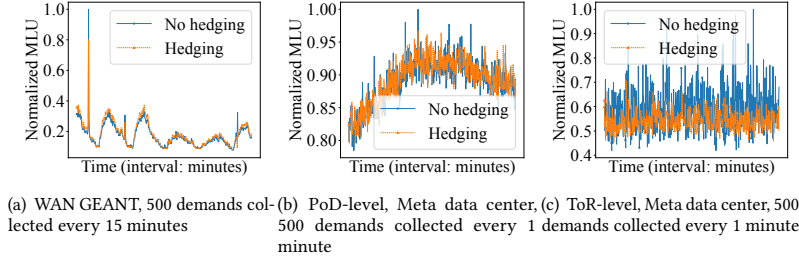


Figure 1: Comparing the impact of using anti-burst Hedging mechanism on maximum link utilization (MLU), with MLU values normalized to the maximum MLU.

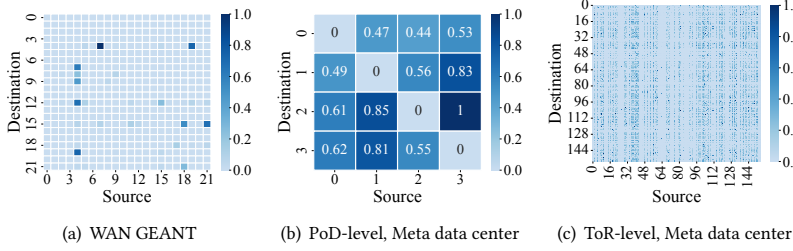


Figure 2: The variance of traffic demand by source and destination (The value of variance has been normalized). The larger the variance, the more likely it is that the traffic demand for that source-destination pair will experience a burst. Regardless of which network in 2(a), 2(b), or 2(c), the traffic demands of different source-destination pairs exhibit different traffic characteristics.

[41] at both the PoD-level and ToR-level. Details on the public data used are provided in §5. For each SD pair, we calculate the variance of the traffic volumes as a measure of the dynamic changes in traffic. The results of our analysis are displayed in Figure 2, which shows the variance of traffic demand for different SD pairs across the three types of network traffic. The greater the variance for a SD pair, the more unstable that SD pair is.

The results in Figure 2 indicate that, regardless of the topology type, the traffic characteristics are distinct for different SD pairs. If one treats the traffic from all the SD pairs equally, the resulting TE solution may either result in suboptimal performance in non-bursty scenarios or sacrifice the burst-handling capability. Hence, effectively leveraging the diverse traffic characteristics in TE is crucial for better balancing the performance trade-off between bursty and non-bursty situations.

2.3 Dig deep into the trade-off

Trade-off dilemma in TE. To illustrate the trade-off dilemma in TE, we present an illustrative example in Figure 3. In this network, there are three traffic demands: $A \rightarrow B$, $A \rightarrow C$, $B \rightarrow C$. In the normal situation, the traffic demand for all three is 1. However, in three different burst situations, the traffic demand for $A \rightarrow B$, $A \rightarrow C$, $B \rightarrow C$ increases to 4, respectively.

TE scheme 1 considers all traffic as non-bursty and only optimizes for the normal situation. To minimize congestion in non-bursty scenarios, TE scheme 1 directs all traffic along the shortest

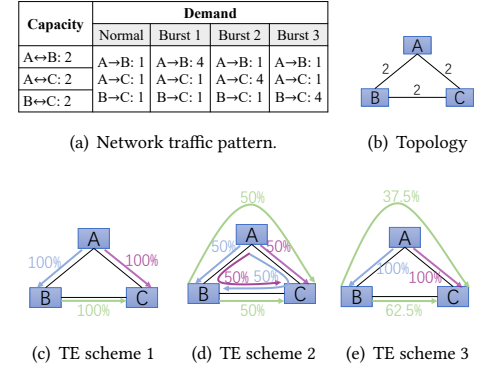


Figure 3: A simple example comparing three TE schemes. TE scheme 1 has the optimal MLU in the normal situation. When traffic burst situations 1/2/3 are all possible, TE scheme 2 exhibits the best resilience against bursts. If only traffic burst situation 3 is likely to occur, TE scheme 3 outperforms TE scheme 2.

paths. In the normal situation, its Max Link Utilization (MLU) is $\max\{\frac{1}{2}, \frac{1}{2}, \frac{1}{2}\} = 0.5$. When any burst situation occurs, the MLU is increased to $\max\{\frac{4}{2}, \frac{1}{2}, \frac{1}{2}\} = 2$.

TE scheme 2 considers all traffic as bursty traffic and aims to enhance robustness in response to the three burst situations by splitting traffic across different paths. When dealing with the normal situation, the MLU of TE scheme 2 is $\max\{\frac{1 \times 0.5 + 1 \times 0.5 + 1 \times 0.5}{2}, \frac{1 \times 0.5 + 1 \times 0.5 + 1 \times 0.5}{2}, \frac{1 \times 0.5 + 1 \times 0.5 + 1 \times 0.5}{2}\} = 0.75$, while dealing with the three burst situations, its MLU is $\max\{\frac{4 \times 0.5 + 1 \times 0.5 + 1 \times 0.5}{2}, \frac{4 \times 0.5 + 1 \times 0.5 + 1 \times 0.5}{2}, \frac{4 \times 0.5 + 1 \times 0.5 + 1 \times 0.5}{2}\} = 1.5$. That is, TE scheme 2 exhibits better robustness in handling traffic bursts compared to TE scheme 1, but with a decrease in normal performance.

Overall, this one-size-fits-all approach either leads to a network lacking the capacity to handle bursts or enhances the capability to manage bursts but at the cost of compromised performance in non-burst situations.

A key insight in balancing normal performance and robustness. We find that a more effective approach is to differentiate treatment based on the unique characteristics of each SD pair. Figure 3(e) illustrates this point. TE scheme 3 specifically addresses the bursts between $B \rightarrow C$, selecting two paths for serving the traffic from B to C. Conversely, for $A \rightarrow B$ and $A \rightarrow C$, it opts for direct paths. In TE scheme 3, the MLU is $\max\{\frac{1 \times 0.375 + 1}{2}, \frac{1 \times 0.375 + 1}{2}, \frac{1 \times 0.625}{2}\} = 0.6875$ under the normal situation. When dealing with the traffic burst situation 1 or 2, the MLU is $\max\{\frac{1 \times 0.375 + 4}{2}, \frac{1 \times 0.375 + 1}{2}, \frac{1 \times 0.625}{2}\} =$

2.1875; when dealing with the traffic burst situation 3, the MLU is $\max\{\frac{4 \times 0.375 + 1}{2}, \frac{4 \times 0.375 + 1}{2}, \frac{4 \times 0.625}{2}\} = 1.25$. It can be observed that, although TE scheme 3 is not as robust as TE scheme 2 in handling traffic burst situation 1/2, it performs better than TE scheme 2 in both normal situations and traffic burst situation 3. If the traffic demand from A to B and A to C never experiences traffic bursts, then TE scheme 3 would be a better solution compared to TE scheme 2. That is, if a traffic demand remains consistently stable, then the robustness of the paths serving that traffic demand does not need to be a concern (similar to how TE scheme 3 does not consider the robustness of path A \rightarrow B and path A \rightarrow C).

Based on the observations in §2.1 and the insights from Figure 2 and Figure 3, it is evident that enhancing robustness to manage unexpected traffic bursts is necessary. However, uniformly increasing the robustness across all paths may lead to a compromise in average performance. A more nuanced strategy would be to adjust the robustness of paths based on the traffic characteristics of the traffic demands they serve. Compared to previous TE methods, this fine-grained robustness enhancement strategy in TE enables a better balance between normal-case performance and burst-case performance.

3 TE MODEL

Notations & Definitions. We introduce recurring mathematical notations and definitions of TE. All notations used in this paper are also tabulated in Table 6 for ease of reference.

- **Network.** We represent the network topology as a graph $G = (V, E, c)$, where V and E are the vertex and edge sets, respectively, and $c : E \rightarrow \mathbb{R}^+$ assigns capacities to edges.
- **Traffic demands.** A Demand matrix (DM) D is a $|V| \times |V|$ matrix whose (i, j) -th entry D_{ij} specifies the traffic demand between source i and destination j .
- **Network paths.** Each source vertex s communicates with each destination vertex d via a set of network paths P_{sd} . We can also say that P_{sd} serves the SD pair (s, d) .
- **Path capacity.** The capacity of a path p is denoted by C_p . It is the minimum capacity across the edges along the path [37].
- **TE configuration.** A TE configuration \mathcal{R} specifies for each source vertex s and destination vertex d how the D_{sd} traffic from s to d is split across the paths in P_{sd} . A TE configuration specifies for each path $p \in P_{sd}$ a split ratio r_p , where r_p is the fraction of the traffic demand from s to d forwarded along path p . The split ratios must satisfy $\sum_{p \in P_{sd}} r_p = 1$.
- **TE objective.** Our TE objective is to minimize the Max Link Utilization (MLU), which is a classical TE objective [10, 11, 17, 37, 48]. Google found MLU to be a reasonable proxy metric for throughput as well as for resilience against traffic pattern variation. They found high MLU indicates many links are in danger of overloading, causing packet losses, increasing flow-completion time, and reducing throughput [37].

Given a demand matrix D and TE configuration \mathcal{R} , the total traffic traversing an edge e is $f_e = \sum_{s,d \in V, p \in P_{sd}, e \in p} D_{sd} \cdot r_p$, and then the MLU induced by D and \mathcal{R} is $\text{MLU} = \max_{e \in E} \frac{f_e}{c(e)}$, which we denote as $M(\mathcal{R}, D)$.

TE under traffic uncertainty. At epoch t , the decision maker in TE must output a network configuration $\mathcal{R}_t(D_1, \dots, D_{t-1})$ based on historical data $\{D_1, \dots, D_{t-1}\}$ before the arrival of D_t . The objective is to obtain a network configuration that yields low link over-utilization for the upcoming traffic D_t .

$$\underset{\mathcal{R}_t(D_1, \dots, D_{t-1})}{\text{minimize}} \quad M(\mathcal{R}_t(D_1, \dots, D_{t-1}), D_t) \quad (1)$$

When configuring \mathcal{R}_t based on historical data $\{D_1, \dots, D_{t-1}\}$ before the arrival of D_t , it is critical to consider both anticipated and unanticipated traffic. An anticipated traffic demand D_t^{expect} can be deduced from historical traffic data using certain traffic prediction technologies. However, we caution that such a prediction may not be accurate due to the existence of highly bursty traffic demands. To attain better network performance, it is crucial to incorporate the mismatch between the predicted traffic demand D_t^{expect} and the real traffic demand D_t when calculating each TE configuration.

4 FIGRET DESIGN

In this section, we present the design of FIGRET. In §4.1, we introduce how FIGRET addresses traffic bursts while solving TE solutions based on historical traffic. Subsequently, §4.2 discusses the transformation of problem-solving into the design of loss functions using deep learning. The design of the loss function and the deep neural network architecture are then detailed in §4.3 and §4.4, respectively. Finally, §4.5 discusses how FIGRET handles node/link failures.

4.1 Design for managing traffic bursts

As outlined in §3, it is not adequate for TE to rely solely on D^{expect} obtained from historical data. To augment robustness, the impact of traffic bursts must be considered.

By defining a set to account for traffic bursts. A prevalent method involves defining the bursts as a set Δ . During the optimization process, the sum of a specific burst $\delta \in \Delta$ and D^{expect} is used as an estimate for the actual traffic, denoted as $\hat{D}_t = \delta + D^{\text{expect}}$. The objective is to find a TE configuration that offers the best worst-case guarantee for all the $\delta \in \Delta$, i.e.,

$$\begin{array}{ll} \underset{\mathcal{R}_t}{\text{minimize}} & \max_{\hat{D}_t \in \hat{\mathcal{D}}} M(\mathcal{R}_t, \hat{D}_t) \\ \text{subject to} & \hat{\mathcal{D}} = \{\hat{D}_t | \hat{D}_t = \delta + D^{\text{expect}}, \delta \in \Delta\} \end{array} \quad (2)$$

Drawback: The above robust optimization based approach could offer varying levels of robustness with different choices of Δ , but still faces the following shortcomings:

- It is hard to find the most appropriate Δ that yields the best trade-off between normal case performance and burst case performance. Although one could use Chebyshev's inequality [33] to quantify a Δ such that the probability $P(D_t \notin \hat{\mathcal{D}})$ is no larger than a small value α , D_t may still go beyond $\hat{\mathcal{D}}$ and the performance guarantee offered by Equation (2) becomes invalid. Admittedly, we could increase Δ such that the probability α is extremely small, but the normal-case performance could then be compromised.
- The objective function in Equation (2) aims to optimize the worst case within the set $\hat{\mathcal{D}}$. Note that $\hat{\mathcal{D}}$ may contain an infinite number of distinct traffic patterns, dramatically increasing the computational complexity of solving Equation (2). In contrast, our

chosen anti-burst strategy in Equation (5) only requires optimization for a single traffic pattern D_t^{expect} .

By imposing constraints to account for traffic bursts. When considering both D^{expect} and δ , the utilization of each edge can be expressed as: $\sum_{s,d \in V, p \in P_{sd}, e \in p} (D_{sd}^{\text{expect}} + \delta_{sd}) \cdot r_p / c(e)$. Consequently, the actual impact of δ_{sd} on each edge can be represented by its coefficient. To mitigate the impact of traffic bursts, we could impose an upper bound on this coefficient. The degree of robustness can be controlled by adjusting the upper bound of each coefficient.

As discussed in §2, we aim to impose varying levels of robustness on different paths based on the traffic characteristics of the SD pairs. Therefore, this constraint should be a function related to the SD pairs, defined as $\mathcal{F} : (s, d) \rightarrow \mathbb{R}^+$.

$$\forall s, d \in V, \forall p \in P_{sd}, \forall e \in p \quad \frac{r_p}{c(e)} \leq \mathcal{F}((s, d)). \quad (3)$$

Considering the definitions of path capacity C_p , as expressed by $C_p = \min_{e \in p} c(e)$, it follows that Equation (3) is equivalent to Equation (4).

$$\forall s, d \in V, \forall p \in P_{st} \quad \frac{r_p}{C_p} \leq \mathcal{F}((s, d)). \quad (4)$$

As indicated in Equation (4), ensuring that the ratio $\frac{r_p}{C_p}$ falls below a certain limit guarantees the robustness of network configurations against burst traffic. Therefore, $\frac{r_p}{C_p}$ can be used as a metric to represent the level of robustness in the network configuration. So we define path sensitivity \mathcal{S}_p for path p as

$$\mathcal{S}_p = \frac{r_p}{C_p}.$$

By taking into account the *path sensitivity* metric in our TE formulation, the impact of traffic bursts can be mitigated. The resulting formulation is shown below:

minimize	$M(\mathcal{R}_t, D_t^{\text{expect}})$	(5)
subject to	$\mathcal{S}_p \leq \mathcal{F}((s, d)), \forall s, d \in V, \forall p \in P_{sd}$	

Remark. In Equation (5), both D_t^{expect} and \mathcal{F} are determined based on historical traffic data $\{D_1, \dots, D_{t-1}\}$. Selecting an appropriate D_t^{expect} and \mathcal{F} for a specific network topology and traffic pattern is not trivial. Existing methods have not finely discriminated between different SD pairs. For example:

- Traditional methods based on direct optimization of MLU after prediction, as well as those based on deep learning [36, 48], set $\mathcal{F}((s, t)) \equiv +\infty, \forall s, t \in V$. They assume that the real flow can be entirely represented by D_t^{expect} . However, due to the inherent dynamic nature of traffic demands, mismatches are inevitable.
- Desensitization-based TE schemes [37] set $\mathcal{F}((s, d)) \equiv \text{const}, \forall s, d \in V$. A single constant value makes it challenging to perfectly balance burst resistance and average performance. Another approach [45] sets \mathcal{S}_p as an objective, aiming to minimize the maximum \mathcal{S}_p among all paths. However, it also does not account for the difference among different SD pairs.

4.2 FIGRET framework

4.2.1 How to compute a TE solution. Given the FIGRET formulation in Equation (5), the next challenge is to efficiently compute TE solutions. Two approaches to consider are the two-stage method and the end-to-end method.

The *two-stage method* first explicitly estimates D_t^{expect} and \mathcal{F} . Then, it employs a linear programming-based algorithm to solve Equation (5). However, this approach has the following shortcomings, making it far from ideal:

- Due to the existence of highly bursty source-destination pairs, predicting a suitable D_t^{expect} is challenging.
- There exists a mismatch between the upstream tasks of determining D_t^{expect} and \mathcal{F} , and the downstream task of optimizing MLU. Predicting D_t^{expect} often relies on Mean Squared Error (MSE) for evaluation, which does not account for network topology—an essential factor in MLU optimization. For instance, in SD pairs with high-capacity paths, the precision of traffic predictions becomes less critical, as illustrated in Figure 19 in Appendix G.1. This oversight can adversely affect TE performance. A similar mismatch affects \mathcal{F} , where constraints should reflect not only traffic characteristics but also the topological structure.
- Employing linear programming involves high computational complexity and may not scale to large networks.

The *end-to-end method* avoids the explicit prediction of D_t^{expect} and \mathcal{F} . Instead, it directly establishes a relationship between historical traffic data $\{D_1, \dots, D_{t-1}\}$ and a TE configuration R_t , with a goal to minimize MLU and ensure robustness. This method's advantage lies in its ability to consider the impact of network topology, eliminating the mismatch between the upstream traffic prediction and the downstream network optimization [36]. Thus, its performance is better than that of the two-stage method (See Appendix C for more details).

Overall, based on the above considerations, we opt for the end-to-end method to compute TE solutions.

4.2.2 Leveraging deep learning to implement the end-to-end method. We employ an end-to-end method to establish a mapping between historical traffic data $\{D_1, \dots, D_{t-1}\}$ and TE configuration R_t that minimizes MLU while ensuring robustness. Since this end-to-end method does not pre-solve D_t^{expect} , we are unable to establish a clear optimization problem as in Equation (5). Therefore, we cannot utilize a linear programming-based approach to implement the end-to-end method. In response, drawing inspiration from DOTE [36], FIGRET adopts a deep neural network (DNN) to implement the end-to-end method. By designing a well-designed burst-aware loss function, FIGRET can output TE solutions that effectively balance normal and burst traffic scenarios.

4.3 Design loss function of FIGRET

In FIGRET, a Deep Neural Network (DNN) is employed to establish a mapping between historical traffic data $\{D_1, \dots, D_{t-1}\}$ and TE configurations. To maintain a consistent input size for the DNN and prevent an overload of traffic data when t is large, a temporal window H is typically chosen [36, 48]. During training, FIGRET receives $\{D_{t-H}, \dots, D_{t-1}\}$, and subsequently outputs a TE Configuration R_t . We denote this output as $R_t = \pi_\theta(D_{t-H}, \dots, D_{t-1})$,

where π represents the mapping function from DNN inputs to outputs, and θ denotes the DNN's link weights. The revealed D_t allows for the calculation of the loss for this R_t through the loss function $\mathcal{L}(R_t, D_t)$, after which a gradient descent optimizer updates the parameters θ . Thus, to enable FIGRET to output TE solutions with fine-grained robustness, a *well-designed loss function* is essential.

The design of our loss function is intrinsically aligned with the Lagrangian relaxation of Equation (5), as delineated in Equation (6). This relaxation framework guides us in structuring a loss function that encompasses two components.

$$\begin{aligned} & \underset{\mathcal{R}_t, \lambda}{\text{minimize}} && L(\mathcal{R}_t, \lambda) = M(\mathcal{R}_t, D_t^{\text{expect}}) \\ & + \sum_{s,d \in V} \sum_{p \in P_{sd}} \lambda_{sd} (\mathcal{S}_p - \mathcal{F}((s,d))) \\ & \text{subject to} && \lambda_{sd} \geq 0, \quad \forall s, d \in V, \forall p \in P_{sd} \end{aligned} \quad (6)$$

4.3.1 Loss for MLU. The first component corresponds to minimizing max link utilization.

$$\mathcal{L}_1 = M(R_t, D_t). \quad (7)$$

With the first loss function in place, upon completion of training, FIGRET *implicitly* learns a probability distribution $P(D_t^{\text{expect}} | D_{t-1}, \dots, D_{t-H})$. It can then output an R_t that optimizes $\mathbb{E}_{D_t^{\text{expect}}} [M(\mathcal{R}_t, D_t^{\text{expect}})]$ with respect to $P(D_t^{\text{expect}} | D_{t-1}, \dots, D_{t-H})$.

4.3.2 Loss for fine-grained robustness. The second component of the loss function reflects the constraints imposed by path sensitivities. Since we adopt an end-to-end TE approach without explicitly solving for $\mathcal{F}((s,d))$ beforehand, we can not directly use the second term of Equation (6)— $\sum_{s,d \in V} \sum_{p \in P_{sd}} \lambda_{sd} (\mathcal{S}_p - \mathcal{F}((s,d)))$ —as the loss function. In response, we design the following heuristic scheme for constructing the second component of the loss.

How to calculate \mathcal{L}_2 ? We use $\sigma_{D_{sd}, [1-T]}^2$ to denote the variance of traffic demands D_{sd} from source s to destination d over the training period from time 1 to T . We denote \mathcal{S}_{sd}^{\max} as the maximum path sensitivity among all paths serving from source s to destination d in the configuration \mathcal{R}_t . Based on this, we can express \mathcal{L}_2 as Equation (8).

$$\mathcal{L}_2 = \sum_{s,d \in V} \sigma_{D_{sd}, [1-T]}^2 \times \mathcal{S}_{sd}^{\max}. \quad (8)$$

How does Equation (8) capture fine-grained robustness? The original term $\sum_{s,d \in V} \sum_{p \in P_{sd}} \lambda_{sd} (\mathcal{S}_p - \mathcal{F}((s,d)))$ facilitates fine-grained robustness because the values of $\mathcal{F}((s,d))$ differ among various source-destination pairs, resulting in different penalties for the same path sensitivity across different paths. To elaborate, for SD pairs with stable traffic patterns, denoted as $(s,d)_{\text{stable}}$, and those characterized by bursty traffic dynamics, labeled as $(s,d)_{\text{bursty}}$, the constraints are more stringent for bursty SD pairs, i.e., $\mathcal{F}((s,d)_{\text{stable}}) > \mathcal{F}((s,d)_{\text{bursty}})$. Therefore, according to $\mathcal{S}_p - \mathcal{F}((s,d))$, the path serving for bursty traffic SD pair incurs a greater penalty. Our design of \mathcal{L}_2 achieves a similar functionality. We calculate the variance of traffic demand $\sigma_{D_{sd}, [1-T]}^2$ for each SD pair from time 1 to T , representing the degree of variation in the

flow. This provides a quantitative measure of traffic fluctuation for the network. Subsequently, we weight these variances with the maximum path sensitivity \mathcal{S}_{sd}^{\max} of paths serving the corresponding SD pair. This approach imposes stricter sensitivity penalties on flows with higher variance and lighter penalties on those with lower variance.

When training the neural network, we consider both the loss term MLU \mathcal{L}_1 and the robustness enhancement term \mathcal{L}_2 . This comprehensive consideration aims to guide the network in learning how to adjust path sensitivity constraints for different SD pairs while maintaining MLU optimization. By this method, we ensure that the network not only meets the MLU optimization objectives but also enhances the burst resistance of different SD pairs in a fine-grained manner.

4.4 Design DNN structure of FIGRET

The structures primarily used in TE are as follows: Graph Neural Network (GNN) [12, 52], Convolutional Neural Network (CNN) [48], and Fully Connected Network (FCN) [36]. In this section, we briefly explain why we chose FCN over GNN and CNN, with more detail available in Appendix D.

Network topology handling: no need for GNN. In TE problems, acquiring and utilizing network topology information is crucial for constructing the mapping between TE configurations and MLU. The network topology $G(V, E, c)$, as a graph structure, seems naturally suited for processing with GNN. However, as Function 1 in Appendix D.1 shows, this mapping relationship can be achieved through simple matrix operations, which can be fully handled by FCN. GNN involves processing based on adjacency matrices and node features, which can lead to redundant computations and higher computational complexity, potentially consuming significant memory [50, 53, 55]. Considering these factors, using FCN seems a more reasonable choice.

CNN vs. FCN: The inappropriateness of CNN. CNN can effectively extract local information in data such as images through convolutional operations. However, in the historical traffic demand data used as input for TE, there is no obvious local information. The traffic sharing a common edge can be spatially close or distant, not necessarily confined to a local area. A detailed example is provided in Figure 13. Therefore, we opted not to use CNN, but rather FCN.

4.5 Coping with node/link failures

In large networks, node/link failures are inevitable, causing some paths unavailable to serve traffic. A widely-adopted approach to addressing network failures in TE involves rerouting traffic around failed paths by allowing traffic sources to proportionally redistribute traffic among their remaining paths [23, 24, 36, 43].

- In cases where the remaining paths have allocation ratios, the traffic demand from a failed path is proportionally redistributed based on these ratios. Consider a scenario with three paths having allocation ratios of (0.5, 0.3, 0.2). If the first path experiences a failure, the adjusted distribution ratios for the remaining paths would be set as (0, 0.6, 0.4).
- Conversely, if the remaining paths do not have allocation ratios, the traffic demand from the failed path is equally distributed among them. For instance, in a situation with three paths at

ratios (1, 0, 0), and the first path fails, the redistributed traffic is allocated evenly, resulting in new ratios of (0, 0.5, 0.5).

We integrate this approach into FIGRET, evaluate its effectiveness, and demonstrate that it achieves high resiliency to failures in §5.3. Notably, handling link failures in FIGRET does not necessitate retraining.

5 EVALUATION

In this section, we evaluate FIGRET. In §5.1, we first describe our evaluation methodology and analyze the types of traffic used in the evaluation to demonstrate that our experiments cover a wide variety of traffic scenarios. Subsequently, in §5.2, we compare FIGRET with state-of-the-art TE schemes, focusing on TE quality, solution times, and precomputation times. Then, the effectiveness of FIGRET in handling link failures and adapting to drifts in traffic patterns is evaluated in §5.3 and §5.4, respectively. Finally, in §5.5, we showcase the fine-grained robustness enhancement capabilities of FIGRET, thereby providing an interpretation of FIGRET's performance.

5.1 Methodology

Topologies. We consider three WAN topologies, including the pan-European research network, GEANT [47], as well as two topologies from the Internet Topology Zoo [29], namely UsCarrier and Kdl. We also examine various data center topologies. This includes the pFabric [8], which utilizes a leaf-spine topology with nine Top-of-Rack (TOR) switches. We change the topology from leaf-spine to a fully connected direct-connect network, because TE is rarely used in leaf-spine topologies. Additionally, we consider two Meta's DC clusters [41]: the Meta DB cluster and the Meta WEB cluster. The Meta DB cluster comprises MySQL servers that store user data and handle SQL queries, whereas the Meta WEB cluster is responsible for serving web traffic. For each cluster, we contemplate two types of topologies: the Top-of-Rack (ToR) level and the Point of Delivery (PoD) level. For Meta's data centers, we also adopt the direct-connect network as the topology. For the PoD level topology, we consider the fully connected network, whereas, for the ToR level topology, we utilize the random regular graph [42]. Their numbers of nodes and edges are summarized in Table 1. For each topology, unless otherwise stated, we employ Yen's algorithm to precompute the three shortest paths between every pair of nodes as the candidate paths for flow allocation [2, 34].

	#Type	#Nodes	#Edges
GEANT	WAN	23	74
UsCarrier	WAN	158	378
Cogentco	WAN	197	486
pFabric	ToR-level DC	9	72
Meta DB	PoD-level DC	4	12
	ToR-level DC	155	7194
Meta WEB	PoD-level DC	8	56
	ToR-level DC	324	31520

Table 1: Network topologies in our evaluation.

Traffic data. For the GEANT topology, there are publicly available traffic matrix traces, which consist of data aggregated every 15 minutes over four months [47]. In the context of pFabric topology, the

pFabric trace is characterized by a Poisson arrival process. When a flow arrives, the source and destination nodes are chosen uniformly at random from the different ToR switches. The size of each flow is determined randomly, adhering to the distribution outlined in the “web search workload” scenario as described in [8]. In the case of the Meta topology, there is a public trace of one day's traffic [41]. For the PoD-level topology, we aggregate traces into 1-second snapshots of the inter-Pod traffic matrix, while for the ToR-level topology, aggregation is performed into 10-second snapshots of the inter-ToR traffic matrix. The longer aggregation time for ToR-level topologies is attributed to their larger scale, which involves more nodes and a more complex network structure, resulting in greater computational and storage demands for TE. For the UsCarrier and Cogentco topologies from Topology Zoo, where no public traffic traces are available, we employ a gravity model [9, 39] to generate synthetic traffic.

Traffic characteristics. Our data includes different types of topologies and their corresponding traffic, each with distinct traffic characteristics. By comparing the similarity of the currently-seen TM with historical TMs, we observe whether the traffic is relatively stable and predictable. Specifically, for every currently-seen TM, we consider a window of historical TMs, find the TMs that most closely resemble this currently-seen TM, and calculate the cosine similarity between the two. Figure 4 shows the distribution of the results. Each candlestick displays the distribution of cosine similarities for different traffics, with the box range extending from the 25th to the 75th percentile. The closer the distribution of a traffic's cosine similarity is to 1, the more similar it is to past traffic, indicating greater stability. Conversely, a cosine similarity closer to 0 suggests that the traffic is more erratic. We can identify the following characteristics:

- The degree of burstiness in traffic increases progressively from WAN traffic to DC POD-level traffic, to DC ToR-level traffic. This may be related to the aggregation of traffic; POD-level traffic aggregates ToR-level traffic, and the WAN connects different data centers, making the aggregation effect more pronounced. The aggregation of multiple traffic streams can cause the bursty variations of different traffic to ‘neutralize’ each other, hence the more aggregation there is, the more stable the traffic becomes.
- Even though WAN traffic is generally stable, there are some anomalies in the cosine similarity distribution of publicly available WAN traffic, indicating that WAN traffic can sometimes experience sudden bursts.
- The WAN traffic generated by the gravity model resembles the trend of real WAN traffic. However, it cannot capture all the characteristics of real traffic, as it fails to reflect traffic bursts. In our experiments, we use it to understand the TE performance in stable traffic conditions.

In summary, the traffic data exhibits various characteristics, including profiles with low, moderate, and high burstiness. This allows for a thorough evaluation of the TE performance in various scenarios.

Baseline. We select the following TE schemes to compare with FIGRET: (1) **Omniscient TE**: This scheme represents an optimization with perfect knowledge of future demands, providing a benchmark for the most efficient performance achievable in all TE schemes. (2) **Desensitization-based TE**: This is the TE scheme used by

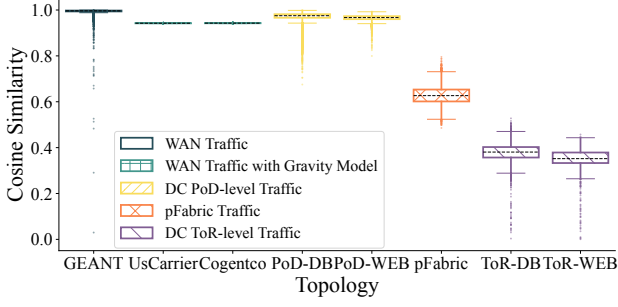


Figure 4: Cosine similarity analysis using a window of 12 historical TMs vs. the currently-seen TM.

Google in Jupiter data center [37] and [44]. This scheme constructs an anticipated matrix composed of the peak values for each source-destination pair within a time window. Then it optimizes the TE objective under the constraint that path sensitivity remains below a predetermined threshold. (3) **Demand-oblivious TE** [9]: This scheme focuses on optimizing the worst-case performance across all possible traffic demands. (4) **Demand-prediction-based TE** [2, 23, 24]: This method involves predicting the next incoming traffic demand and configuring accordingly, *without* considering the mis-predictions that may arise from the traffic uncertainty. (5) **COPE** [49]: This scheme enhances demand-oblivious TE by also optimizing over a set of predicted traffic demands. It optimizes MLU across a set of DMs predicted based on previously observed DMs while retaining a worst-case performance guarantee. (6) **Deep Learning-based TE (DOTE)** [36]: DOTE employs a DNN to directly output the TE configuration based on the traffic demand observed within a given time window. (7) **TEAL** [52]: TEAL employs a combination of GNN and Reinforcement Learning (RL) to process a given traffic demand, subsequently outputting a network configuration tailored for this demand. In our experiments, due to the absence of prior knowledge about future traffic, we apply the TE solution computed from the traffic demand of the preceding time snapshot to the next time snapshot. (8) **SMORE** [31]: SMORE employs Racke’s oblivious routing paths [38] for path selection, with traffic splitting ratios optimized for the predicted future traffic demands.

Infrastructure and software. Our experiments are carried out on an Intel(R) Xeon(R) Silver 4110 CPU, equipped with 128GB of memory. Furthermore, Nvidia-Tesla P100 GPUs are accessible for all schemes, but only FIGRET, DOTE, and TEAL can utilize them. We implement FIGRET using PyTorch [35]. For detailed information on neural network architecture, parameters, and optimizer settings, please refer to Appendix D. For TE schemes that necessitate solving optimization problems, Gurobi (version 9.5.2) [21] is employed.

5.2 Comparing with other TE schemes

TE quality. Figure 5 compares the quality of TE solutions between FIGRET and other TE schemes. The y-axis value represents the MLU normalized by that of the Omniscient TE. We note the findings:

- **Desensitization-based TE.** Across all topologies, the performance of Desensitization-based TE in terms of both normal-case MLU (represented by the box) and the worst-case MLU (indicated

by the top of the upper dashed line) is not satisfactory. This is due to the fact that Desensitization-based TE imposes unnecessary path sensitivity constraints on non-bursty traffic while providing insufficient path sensitivity constraints for bursty traffic. We will more clearly illustrate this using Figure 8 in §5.5.

- **Demand-prediction-based TE.** Demand-prediction-based TE methods primarily excel in environments with stable traffic demands. However, their effectiveness significantly diminishes when unexpected traffic bursts occur. The performance of these methods is highly dependent on the accuracy of traffic demand predictions.
- **Demand-oblivious TE & COPE.** Due to the extensive computation time and memory requirements of Demand-oblivious TE and COPE, we can only evaluate a few smaller-scale topologies. The two methods for handling mis-prediction are essentially the use of a set-based approach as introduced in §4.1. It is evident that selecting a set not only increases computational complexity but also makes it difficult to achieve a good balance between normal-case performance and robustness to traffic bursts.
- **DOTE.** DOTE, the best-performing algorithm in existing TE [36], leverages deep learning to map historical traffic data with the next network configurations, achieving outstanding normal-case performance. DOTE implicitly learns to achieve the lowest expected MLU with D^{expect} , reaching the optimal average performance among existing methods. However, its drawback lies in handling burst situations. For example, in the GEANT data, as shown in Figure 4, while most of the data points have high cosine similarity, close to 1, there are some outliers where the traffic’s cosine similarity with past window traffic is very low, representing the unexpected burst scenarios cases. This leads to DOTE’s MLU performance on GEANT data being close to that of Omniscient in most situations but with some peak values. As illustrated in Figure 5(b), in ToR-level DC with high dynamic characteristics, DOTE performs worse than FiGRET in terms of both average performance and robustness.
- **TEAL.** TEAL is designed to train a fast and scalable TE scheme. It receives a traffic demand and outputs a network configuration specifically for this demand. However, when this network configuration is applied to traffic demands with unexpected bursts, it tends to underperform.
- **FIGRET.** Our designed FIGRET achieves better results than previous TE methods, striking a better balance between normal-case performance and burst-case performance. For instance, compared to the TE scheme currently in Google’s production data center network, FIGRET reduces the average MLU by 9%-34%. Against the state-of-the-art DOTE algorithm, FIGRET achieves a reduction in average MLU of 4.5% and 5.3% on ToR-level Meta DB and ToR-level Meta WEB, respectively, both characterized by high traffic dynamics. Even in stable topologies like WAN or Pod-level Datacenters, FIGRET performs no worse than DOTE. Simultaneously, we consider situations where the normalized MLU is greater than 2 as instances of severe congestion caused by inadequate network configuration. For the ToR-level Meta DB, FIGRET exhibits a 41% lower incidence of severe congestion compared to DOTE, while for the ToR-level Meta WEB, the reduction is 53.9%.

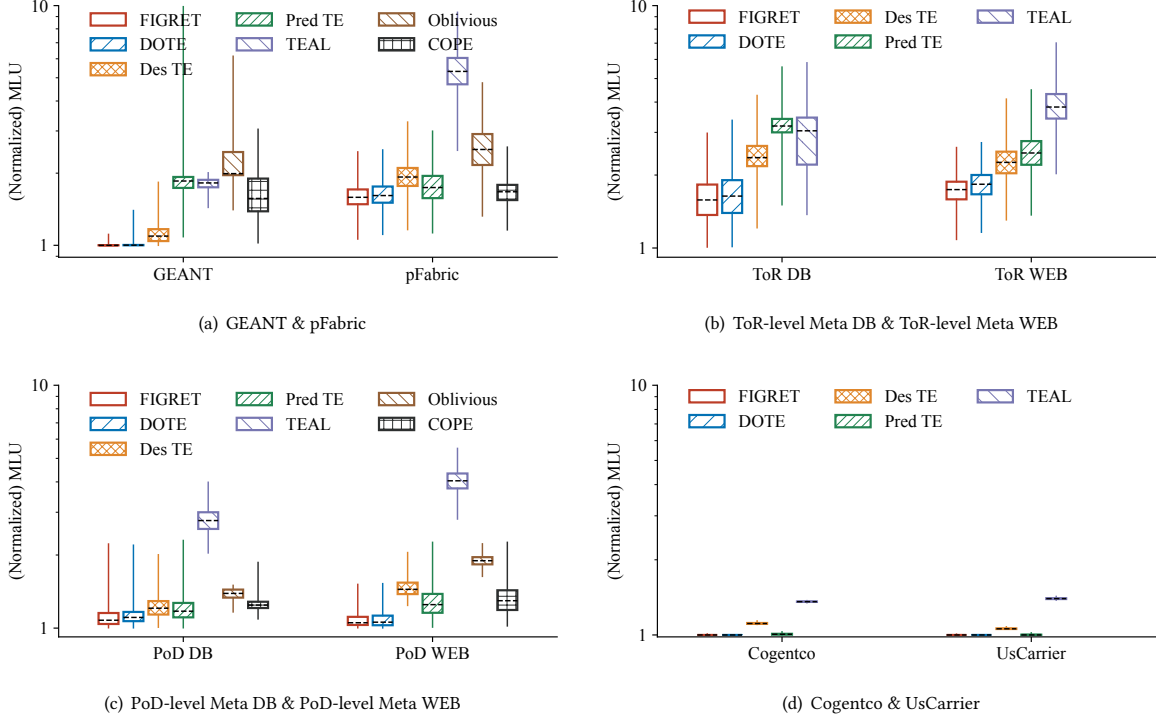


Figure 5: Performance of FIGRET and baselines under the objective of minimizing max link utilization (MLU). The y-axis value represents the MLU normalized by that of the Omniscent TE.

Furthermore, as shown in Figure 5(d), all TE methods exhibit a low normalized MLU with no peaks. This is because the synthetic traffic generated by the gravity model is very stable and lacks traffic bursts. That said, handling traffic bursts is still critical for real WAN traffic because real WAN traffic does contain unexpected bursts.

Solver time. The solver time consists of two parts: the calculation time required to compute a new TE scheme for each new demand matrix, and the precomputation time. Table 2 presents a comparison of the calculation time for different TE schemes. Table 2 lists four items: 1) FIGRET, 2) a Linear Programming (LP) approach that optimizes solely for expected traffic demands without applying any anti-burst strategy, 3) Desensitization-based TE, which handles traffic bursts by limiting path sensitivity, and 4) Oblivious & COPE, which precompute TE solutions but do not update them thereafter; hence, we only test whether they can solve a problem instance. Clearly, FIGRET has the smallest calculation time, while Oblivious & COPE TE schemes have the poorest scalability, failing to compute a solution for larger networks. The comparison between LP and Des TE shows that adding the path sensitivity constraints to handle traffic bursts increases the LP solver calculation time. In contrast, thanks to the adoption of deep neural network, FIGRET is able to enhance robustness without increasing solver complexity. Compared to Des TE, FIGRET achieves a speed-up of 35× to 1800×.

Regarding the training time, since we employ a simple FCN architecture in FIGRET, the precomputation time required is shorter than COPE and reinforcement learning-based TE, especially when

dealing with large-scale topologies. COPE and Demand-oblivious require substantial precomputation latency and a significant amount of memory. Given a maximum runtime of 1 day and machine memory constraints, they only completed the topologies for GEANT, pFabric, and Pod-level DC. Past public results also show their applicability is limited to smaller topologies [36, 49]. Simultaneously, compared to TEAL, which employs reinforcement learning and graph neural networks, FIGRET also has advantages in terms of training time. Detailed data are presented in Table 2.

Path selection. We compare FIGRET with SMORE. SMORE uses a set of paths computed by Räcke’s oblivious routing algorithm. To ensure fairness, we use the same Räcke’s routing algorithm to generate paths for other algorithms. In this case, the prediction-based TE coincides with SMORE. The results are summarized in Figure 6. Again, FIGRET demonstrates the best performance among all the TE algorithms. By comparing Figure 6 and Figure 5(a), it is evident that path selections do not fundamentally affect the effectiveness of different TE schemes. SMORE aims to enhance the robustness merely through path selection. After the paths have been determined, SMORE optimizes the TE performance based solely on the predicted traffic, without considering the potential traffic bursts. As shown by the Pred TE results in the GEANT network in Figure 6, SMORE incurs the highest tail normalized MLU among all the TE schemes. This indicates that merely enhancing TE robustness through path selection is insufficient.

Network	Calculation time (s)				Precomp. time (s)			
	FIGRET	LP	Des TE	Oblivious & Cope	FIGRET	TEAL	Oblivious	COPE
GEANT (#Nodes 23, #Edges 74)	0.002	0.04	0.07	Feasible	150	1500	100	1000
ToR DB (#Node 155, #Edges 7194)	0.005	1.60	5.00	Infeasible	500	7000	-	-
ToR WEB (#Node 324, #Edges 31520)	0.009	7.30	17.00	Infeasible	1500	20000	-	-

Table 2: Comparing the calculation and precomputation time across various TE schemes.

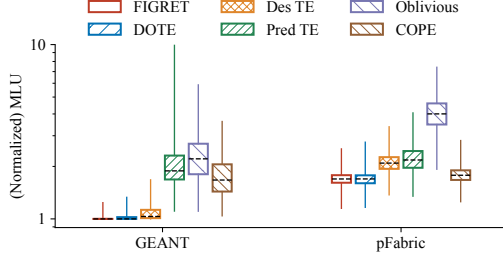


Figure 6: Performance of FIGRET and baselines with routing paths chosen by SMORE. “Pred TE” represents SMORE.

5.3 Coping with network failures

Figure 7 shows the performance of FIGRET, when different numbers of randomly selected links fail within the GEANT topology. We conduct a comparison between FIGRET, DOTE, Desensitization-based TE (Des TE), and Des TE that is also fault-aware (FA Des TE). Fault-aware refers to knowing the links that will fail in the *future* and optimizing only over the paths without failures, without the need to reroute the traffic around failed paths after the TE solutions are determined. Their result is normalized against an oracle that possesses the best knowledge of both future demands and failures. Our results demonstrate that FIGRET achieves high resiliency to link failures. It outperforms both the DOTE and Des TE and is equally competitive with the FA Des TE, which has Oracle access to future failures. Our interpretation for this is that first, compared to DOTE, FIGRET, by incorporating robustness constraints, ensures that the traffic load on a path does not become excessive, thereby mitigating the impact of link failures on performance. The reason why FIGRET achieves comparable performance with FA Des TE is twofold: firstly, Des TE’s explicit prediction of the traffic matrix introduces errors; secondly, it lacks fine-grained robustness enhancement. These factors offset the advantage FA Des TE gains from knowing link failures. Our results on other topologies are presented in Appendix E. These additional results also exhibit similar characteristics.

5.4 Robustness to demand changes

Temporal changes in traffic. We test FIGRET for traffic variability. Our method for increasing variability is as follows: For each source-destination (SD) pair in the real traffic, we generate a traffic fluctuation using the Gaussian distribution $N(\mu, \sigma^2)$ multiplied by a factor α , where $\mu = 0$ and σ is the standard deviation of the traffic demand d_{st} . Here, α is chosen from the set $\{0.2, 0.5, 1.0, 2.0\}$, indicating the amplitude of the fluctuation. We observe how much the performance of FIGRET decreased after imposing sudden traffic

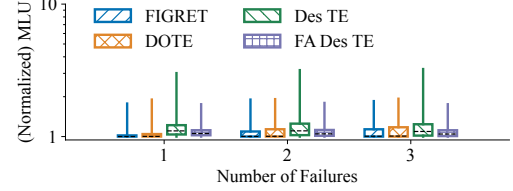


Figure 7: Coping with different numbers of random link failures on GEANT.

changes, compared to its performance without such changes. The results are summarized in Table 3. It can be observed that when the factor α is relatively small, there is no significant decrease in FIGRET’s performance. At the same time, when the factor α is 2, doubling the noise of $N(0, \sigma_{D_{sd}, [1-T]}^2)$, the performance does not decrease by more than 20%.

Natural drift in traffic. We test the impact of natural traffic shifts on FIGRET. In the aforementioned experiment, we sorted the data chronologically, using the first 75% for training and the latter 25% for testing. However, in this section, we conduct training separately with 0%-25%, 25%-50%, and 50%-75% of the data, followed by testing on the last 25%. This approach allows us to observe the performance decline compared to when 75% of the data is used for training. We focus on two aspects: firstly, the impact of training with less data on FIGRET’s performance; secondly, the effect of the update frequency on performance. The results are summarized in Table 4. It is observed that FIGRET’s performance remains largely unaffected even a long time after training completion (exceeding two times the total duration of the training data). To fully understand how traffic data evolves across time, we also visually analyzed the data distribution across various times, presented in Appendix F. The analysis indicates that neither PoD-level nor ToR-level data exhibit drastic changes in their traffic patterns over time. However, the shift effect at the ToR level is somewhat more pronounced than at the PoD level. This corresponds with our results in Table 4. Through this analysis, we are inspired that the FIGRET training does not necessarily need to be especially frequent.

Worst-case performance. We evaluate the performance of FIGRET under worst-case conditions. Considering that FIGRET develops strategies based on the characteristics of historical data, we intentionally reverse the order of the magnitude of temporal traffic fluctuations among SD pairs, applying larger traffic fluctuations to those pairs with historically lower variances. The results are summarized in Table 5. Compared to the results in Table 3, although there is indeed a greater decline in FIGRET’s performance, with PoD DB and ToR DB experiencing a 30%-40% reduction when $\alpha = 2$, the performance did not completely fail. Additionally, we employ

Network		Factor α			
		0.2	0.5	1.0	2.0
PoD DB	average	-0.3%	0.2%	3.2%	9.8%
	90th Pct.	2.0%	3.0%	6.6%	16.7%
pFabric	average	0.2%	-0.6%	-1.8%	-2.9%
	90th Pct.	0.4%	0.5%	-1.0%	1.0%
ToR DB	average	1.6%	3.9%	8.9%	16.1%
	90th Pct.	0.8%	2.8%	4.5%	5.3%

Table 3: Performance decline with increased traffic fluctuation. Negative values indicate no degradation.

Network		Training data time segments		
		0%-25%	25%-50%	50%-75%
PoD DB	average	-0.6%	-0.4%	-0.4%
	90th Pct.	-0.6%	-0.0%	-0.7%
pFabric	average	0.6%	0.9%	0.6%
	90th Pct.	1.3%	0.2%	1.0%
ToR DB	average	2.5%	2.0%	2.5%
	90th Pct.	3.0%	1.6%	1.6%

Table 4: Performance decline with natural drift in traffic. Negative values indicate no degradation.

Network		Factor			
		0.2	0.5	1.0	2.0
PoD DB	average	-0.3%	0.7%	4.8%	15.3%
	90th Pct.	1.7%	1.0%	6.6%	27.9%
pFabric	average	0.2%	-0.6%	-1.7%	-2.7%
	90th Pct.	0.5%	0.7%	-0.4%	1.6%
ToR DB	average	0.9%	2.7%	17.0%	38.6%
	90th Pct.	0.0%	2.6%	23.1%	32.4%

Table 5: Performance decline under worst-case conditions. Negative values indicate no degradation.

the Spearman rank correlation coefficient to assess the consistency of variance ranking changes between the test and train sets across different SD pairs within our dataset. The analysis reveals a high Spearman rank correlation coefficient, with PoD DB at 0.92 and ToR DB at 0.98. These results suggest that the actual occurrence of the worst-case scenario we are considering is rare. Furthermore, for the pFabric system, since the sources and destinations of traffic are selected through a uniform random process, the differences in variance among SD pairs are not pronounced. Therefore, the performance variations are not significant.

5.5 Interpreting FIGRET’s effectiveness

Beyond the impressive end-to-end results achieved by FIGRET, we aim to provide a high-level explanation that is easily understandable to humans. In this way, we aim to make network operators more inclined to implement FIGRET in practice.

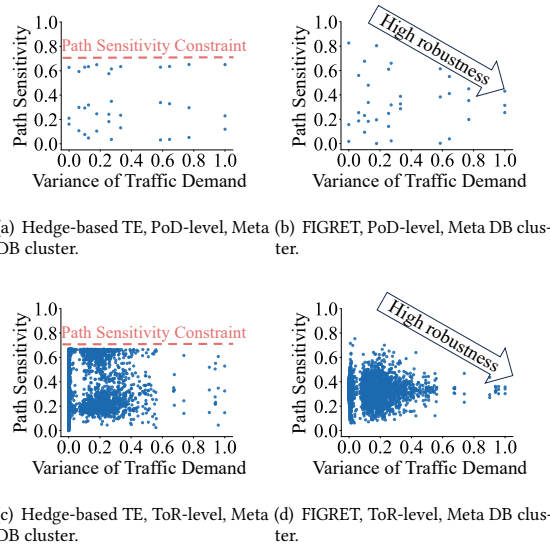


Figure 8: Compare the distribution of path sensitivities in Hedge-based TE with FIGRET. Each point in the graph represents a path, with the x-axis indicating the variance of the traffic served by that path. The y-axis represents the average sensitivity of the path across all tested traffic demands.

Sensitivity analysis in FIGRET. We numerically examine how FIGRET achieves fine-grained robustness. We compare the network configurations of Google’s hedge-based TE and FIGRET, examining the relationship between path sensitivity and traffic characteristics. The results are presented in Figure 8. When creating Figure 8, we normalize the variance of the traffic on the x-axis. For the y-axis, when calculating path sensitivity, we normalize the capacity of the edges (considering the edge with the smallest capacity in the topology as 1). Furthermore, for the ToR level topology in Figure 8(c) and 8(d), with 155 nodes representing 155×154 SD pairs and three paths per SD pair, there are a total of 1551543 paths. Due to the excessive number of points to plot, we uniformly select 10% of the SD pairs for better visualization. From these results, we have the following observations: 1) For hedge-based TE, the path sensitivity of all paths, whether traffic is bursty or not, is constrained within a constant upper bound. 2) For FIGRET, path sensitivity settings depend on traffic characteristics: it’s dispersed for non-bursty and concentrated for bursty traffic. This enables fine-grained robustness analysis, achieving a better balance between normal-case performance and robustness to burst traffic.

6 DISCUSSION

Is deep learning essential for implementing the concept of fine-grained robustness enhancement? In the design of FIGRET, we harness deep learning to devise a robustness enhancement scheme based on complex traffic characteristics and network topologies. However, considering that commercial network operators may be reluctant to overhaul their existing in-production TE systems completely, we discuss in this section whether slight modifications to the existing TE schemes, incorporating the principles of robustness enhancement, could result in better performance compared to the original TE schemes. To investigate this, we make slight modifications to the TE system currently in use by Google’s Jupiter data centers. We discover that by designing simple heuristic-based \mathcal{F} path sensitivity constraint functions that align with fine-grained robustness concepts, the performance of TE algorithms can be improved. We use linear functions to impose stricter constraints as traffic variability increases. We also use piecewise functions to divide traffic into more stable and bursty segments, applying looser constraints to stable segments and stricter constraints to bursty segments. We validate that even such simple functions can improve the original TE’s performance. For example, when using linear functions, if we maintain the constraints for high bursty traffic but relax the constraints for low bursty traffic, we can achieve a 5% reduction

in the average normal-case MLU while maintaining robustness (see Appendix C for more details).

Although it is feasible to directly apply fine-grained robustness enhancements to traditional TE systems currently in operation, this approach encounters two significant issues: firstly, the use of LP methods for solving is notably slow. Secondly, manually configured functions often fall short of achieving optimal performance due to their inability to fully adapt to complex networks and dynamic traffic demands. Given these considerations, this paper employs a method based on deep learning.

When should FIGRET be retrained? In this paper, FIGRET adopts a relatively simple periodic retraining approach, and as demonstrated in §5.4, retraining does not necessarily have to be particularly frequent. Thanks to FIGRET's rapid training times, this periodic training approach can meet usage requirements. Alternative methods, such as retraining after detecting significant changes in network traffic patterns or a certain degree of performance degradation, might more accurately determine the timing for retraining. However, we leave these considerations for future work.

Is it feasible to deploy deep learning-based TE methods in practice? In general, there are two main obstacles that may prevent the practical deployment of deep learning-based methods: 1) the learning-based methods may sometimes produce incorrect or infeasible solutions, and 2) the performance results are not easily interpretable, raising concerns about the solution reliability in different cases. Nevertheless, we argue that the above issues are less of a concern for FIGRET. First, the constraints of TE, which require that the sum of proportions served by all paths for a given source-destination pair equals one, can be easily enforced by normalizing the outputs of the neural network, thus avoiding infeasible solutions. Second, FIGRET's superior performance is explainable, as demonstrated in §5.5.

Can the concept of fine-grained robustness be extended to other objectives? Firstly, fine-grained robustness in traffic not only applies to minimizing MLU but can also be extended to other objectives such as minimizing latency. For instance, selecting the shortest path for non-burst traffic can achieve minimal latency; however, for potential burst traffic, employing multipath transmission may be necessary to avoid congestion on the shortest paths. Secondly, the concept of fine-grained robustness is also applicable to handling link failures. Existing strategies, such as FFC [32], often optimize for all possible failure scenarios, which can lead to low utilization and over-provisioning. By adopting a fine-grained approach that considers the probability of failure scenarios, resource utilization, and fault management can be balanced more effectively.

7 RELATED WORK

Robustness-enhanced-based TE. A major focus of research on TE is to improve the algorithm's robustness in handling sudden traffic bursts. Oblivious TE [9] aims to enhance robustness by consistently considering the most congested scenario, optimizing for the worst-case MLU among all possible DMs. COPE [49] optimizes MLU across a set of DMs predicted by historical DMs while holding a worst-case MLU guarantee. Desensitization-based TE [37, 44], by introducing the concept of path sensitivity which characterizes

the impact of traffic bursts on the path, aims to enhance robustness by optimizing the MLU while ensuring low path sensitivity. Robustness-enhanced TE schemes typically exhibit coarse granularity by treating each source-destination pair in the traffic matrix equally. In contrast, FIGRET stands apart by employing fine-grained robustness enhancement, resulting in a better balance between robustness and average-case performance.

Threshold-based VLB Routing: TROD [14, 15] introduces a threshold-based routing strategy in optical data centers to handle unexpected traffic bursts. The basic idea is that when traffic demand is below a predetermined threshold, the traffic is routed via shortest paths. When traffic demand exceeds the threshold, the burst traffic is load-balanced across all non-shortest paths. TROD maintains normal-case performance by routing most traffic via the shortest paths, while it enhances robustness by dispersing bursts across multiple paths. Hence, TROD strikes a good balance between normal-case and worst-case performance. Unfortunately, TROD's routing algorithm requires special hardware support. P4 switches can support TROD's routing algorithm, but they are not widely deployed in data centers. In contrast, FIGRET does not require specialized hardware and only needs switches that support WCMP.

Machine learning-based TE. Machine learning-based TE can be broadly categorized into two classes. The first class is Demand Prediction-based TE [1, 31, 35, 36]. These methods use predictive models to estimate the next traffic matrix (TM) and then perform optimization based on the estimated TM. The second class replaces explicit demand prediction with end-to-end optimization, directly mapping a recent historical window of TMs to TE configurations [36, 48]. Despite harnessing the powerful capabilities of deep learning to learn relationships between traffic flows, both of these classes overlook the consideration of unexpected traffic bursts.

Network planning. The objective of network planning is to configure network capacity to ensure good performance for all possible traffic patterns. Consequently, Meta models the traffic based on the Hose model [4, 18] and optimizes for the worst-case performance. This approach is not directly applicable to TE because it adjusts network capacity rather than routing weights on paths. Furthermore, even if one may repurpose a network planning approach to solve TE problems, the resulting solution lacks the capability to balance normal-case performance and burst-case performance.

8 CONCLUSION

In this work, we introduce FIGRET, a new design point for TE that enhances robustness in a fine-grained manner based on traffic characteristics. FIGRET employs path sensitivity to manage traffic bursts and utilizes a deep learning strategy with a well-designed loss function to produce TE solutions that consider robustness at a fine-grained level. Our experimental results demonstrate that FIGRET achieves an effective balance between normal-case performance and robustness, resulting in high-quality TE solutions.

ACKNOWLEDGMENTS

We sincerely thank our shepherd Manya Ghobadi and the anonymous reviewers for their constructive feedback. This work was supported by the NSF China (No. 62272292, No. 62132009 and No. 61960206002).

REFERENCES

- [1] 2024. Github repository containing our code. <https://github.com/FIGRET/figret.git>
- [2] Firas Abuzaid, Srikanth Kandula, Behnaz Arzani, Ishai Menache, Matei Zaharia, and Peter Bailis. 2021. Contracting wide-area network topologies to solve flow problems quickly. In *18th USENIX Symposium on Networked Systems Design and Implementation (NSDI 21)*. 175–200.
- [3] Sugam Agarwal, Murali Kodialam, and TV Lakshman. 2013. Traffic engineering in software defined networks. In *2013 Proceedings IEEE INFOCOM*. IEEE, 2211–2219.
- [4] Satyajet Singh Ahuja, Varun Gupta, Vinayak Dangui, Soshant Bali, Abishek Gopalan, Hao Zhong, Petr Lapukhov, Yiting Xia, and Ying Zhang. 2021. Capacity-efficient and uncertainty-resilient backbone network planning with hose. In *Proceedings of the 2021 ACM SIGCOMM 2021 Conference*. 547–559.
- [5] Ian F Akyildiz, Ahyoung Lee, Pu Wang, Min Luo, and Wu Chou. 2014. A roadmap for traffic engineering in SDN-OpenFlow networks. *Computer Networks* 71 (2014), 1–30.
- [6] Mohammad Al-Fares, Sivasankar Radhakrishnan, Barath Raghavan, Nelson Huang, Amin Vahdat, et al. 2010. Hedera: dynamic flow scheduling for data center networks. In *Nsdi*, Vol. 10. San Jose, USA, 89–92.
- [7] Mohammad Alizadeh, Tom Edsall, Sarang Dharmapurikar, Ramanan Vaidyanathan, Kevin Chu, Andy Fingerhut, Vinh The Lam, Francis Matus, Rong Pan, Navindra Yadav, et al. 2014. CONGA: Distributed congestion-aware load balancing for datacenters. In *Proceedings of the 2014 ACM conference on SIGCOMM*. 503–514.
- [8] Mohammad Alizadeh, Shuang Yang, Milad Sharif, Sachin Katti, Nick McKeown, Balaji Prabhakar, and Scott Shenker. 2013. pfabric: Minimal near-optimal data-center transport. *ACM SIGCOMM Computer Communication Review* 43, 4 (2013), 435–446.
- [9] David Applegate and Edith Cohen. 2003. Making intra-domain routing robust to changing and uncertain traffic demands: Understanding fundamental tradeoffs. In *Proceedings of the 2003 conference on Applications, technologies, architectures, and protocols for computer communications*. 313–324.
- [10] Yossi Azar, Edith Cohen, Amos Fiat, Haim Kaplan, and Harald Racke. 2003. Optimal oblivious routing in polynomial time. In *Proceedings of the thirty-fifth annual ACM symposium on Theory of computing*. 383–388.
- [11] Theophilus Benson, Ashok Anand, Aditya Akella, and Ming Zhang. 2011. MicroTE: Fine grained traffic engineering for data centers. In *Proceedings of the seventh conference on emerging networking experiments and technologies*. 1–12.
- [12] Guillermo Bernárdez, José Suárez-Varela, Albert López, Bo Wu, Shiha Xiao, Xiang Cheng, Pere Barlet-Ros, and Albert Cabellos-Aparicio. 2021. Is machine learning ready for traffic engineering optimization?. In *2021 IEEE 29th International Conference on Network Protocols (ICNP)*. IEEE, 1–11.
- [13] Jeremy Bogle, Nikhil Bhatia, Manya Ghobadi, Ishai Menache, Nikolaj Bjørner, Asaf Valadarsky, and Michael Schapira. 2019. TEAVAR: striking the right utilization-availability balance in WAN traffic engineering. In *Proceedings of the ACM Special Interest Group on Data Communication*. 29–43.
- [14] Peirui Cao, Shizhen Zhao, Min Yee Teh, Yunzhuo Liu, and Xinbing Wang. 2021. TROD: Evolving From Electrical Data Center to Optical Data Center. In *2021 IEEE 29th International Conference on Network Protocols (ICNP)*. IEEE, 1–11.
- [15] Peirui Cao, Shizhen Zhao, Dai Zhang, Zhuotao Liu, Mingwei Xu, Min Yee Teh, Yunzhuo Liu, Xinbing Wang, and Chenghu Zhou. 2023. Threshold-based routing-topology co-design for optical data center. *IEEE/ACM Transactions on Networking* (2023).
- [16] Li Chen, Justinas Lingys, Kai Chen, and Feng Liu. 2018. Auto: Scaling deep reinforcement learning for datacenter-scale automatic traffic optimization. In *Proceedings of the 2018 conference of the ACM special interest group on data communication*. 191–205.
- [17] Marco Chiesa, Gábor Rétvári, and Michael Schapira. 2016. Lying your way to better traffic engineering. In *Proceedings of the 12th International on Conference on emerging Networking EXperiments and Technologies*. 391–398.
- [18] John P Eason, Xueqi He, Richard Cziva, Max Noormohammadpour, Srivatsan Balasubramanian, Satyajet Singh Ahuja, and Biao Lu. 2023. Hose-based cross-layer backbone network design with Benders decomposition. In *Proceedings of the ACM SIGCOMM 2023 Conference*. 333–345.
- [19] Anwar Elwalid, Cheng Jin, Steven Low, and Indra Widjaja. 2001. MATE: MPLS adaptive traffic engineering. In *Proceedings IEEE INFOCOM 2001. Conference on Computer Communications. Twentieth Annual Joint Conference of the IEEE Computer and Communications Society (Cat. No. 01CH37213)*, Vol. 3. IEEE, 1300–1309.
- [20] Bernard Fortz and Mikkel Thorup. 2000. Internet traffic engineering by optimizing OSPF weights. In *Proceedings IEEE INFOCOM 2000. conference on computer communications. Nineteenth annual joint conference of the IEEE computer and communications societies (Cat. No. 00CH37064)*, Vol. 2. IEEE, 519–528.
- [21] LLC Gurobi Optimization. 2021. Gurobi optimizer reference manual.
- [22] Geoffrey E Hinton and Sam Roweis. 2002. Stochastic neighbor embedding. *Advances in neural information processing systems* 15 (2002).
- [23] Chi-Yao Hong, Srikanth Kandula, Ratul Mahajan, Ming Zhang, Vijay Gill, Mohan Nanduri, and Roger Wattenhofer. 2013. Achieving high utilization with software-driven WAN. In *Proceedings of the ACM SIGCOMM 2013 Conference on SIGCOMM*. 15–26.
- [24] Sushant Jain, Alok Kumar, Subhasree Mandal, Joon Ong, Leon Poutievski, Arjun Singh, Subbaiah Venkata, Jim Wanderer, Junlan Zhou, Min Zhu, et al. 2013. B4: Experience with a globally-deployed software defined WAN. *ACM SIGCOMM Computer Communication Review* 43, 4 (2013), 3–14.
- [25] Wenjie Jiang, Rui Zhang-Shen, Jennifer Rexford, and Mung Chiang. 2009. Co-operative content distribution and traffic engineering in an ISP network. In *Proceedings of the eleventh international joint conference on Measurement and modeling of computer systems*. 239–250.
- [26] Srikanth Kandula, Dina Katabi, Bruce Davie, and Anna Charny. 2005. Walking the tightrope: Responsive yet stable traffic engineering. *ACM SIGCOMM Computer Communication Review* 35, 4 (2005), 253–264.
- [27] Srikanth Kandula, Ishai Menache, Roy Schwartz, and Spandana Raj Babbula. 2014. Calendaring for wide area networks. In *Proceedings of the 2014 ACM conference on SIGCOMM*. 515–526.
- [28] Diederik P Kingma and Jimmy Ba. 2014. Adam: A method for stochastic optimization. *arXiv preprint arXiv:1412.6980* (2014).
- [29] Simon Knight, Hung X Nguyen, Nickolas Falkner, Rhys Bowden, and Matthew Roughan. 2011. The internet topology zoo. *IEEE Journal on Selected Areas in Communications* 29, 9 (2011), 1765–1775.
- [30] Alok Kumar, Sushant Jain, Uday Naik, Anand Raghuraman, Nikhil Kasinadhuni, Enrique Cauich Zermeno, C Stephen Gunn, Jing Ai, Björn Carlin, Mihai Amarandei-Stavila, et al. 2015. BwE: Flexible, hierarchical bandwidth allocation for WAN distributed computing. In *Proceedings of the 2015 ACM Conference on Special Interest Group on Data Communication*. 1–14.
- [31] Praveen Kumar, Yang Yuan, Chris Yu, Nate Foster, Robert Kleinberg, Petr Lapukhov, Chiun Lin Lim, and Robert Soule. 2018. {Semi-Oblivious} Traffic Engineering: The Road Not Taken. In *15th USENIX Symposium on Networked Systems Design and Implementation (NSDI 18)*. 157–170.
- [32] Hongqiang Harry Liu, Srikanth Kandula, Ratul Mahajan, Ming Zhang, and David Gelernter. 2014. Traffic engineering with forward fault correction. In *Proceedings of the 2014 ACM Conference on SIGCOMM*. 527–538.
- [33] Albert W Marshall and Ingram Olkin. 1960. Multivariate chebyshev inequalities. *The Annals of Mathematical Statistics* (1960), 1001–1014.
- [34] Deepak Narayanan, Fiodar Kazhamiaka, Firas Abuzaid, Peter Kraft, Akshay Agrawal, Srikanth Kandula, Stephen Boyd, and Matei Zaharia. 2021. Solving large-scale granular resource allocation problems efficiently with pop. In *Proceedings of the ACM SIGOPS 28th Symposium on Operating Systems Principles*. 521–537.
- [35] Adam Paszke, Sam Gross, Francisco Massa, Adam Lerer, James Bradbury, Gregory Chanan, Trevor Killeen, Zeming Lin, Natalia Gimelshein, Luca Antiga, et al. 2019. Pytorch: An imperative style, high-performance deep learning library. *Advances in neural information processing systems* 32 (2019).
- [36] Yarin Perry, Felipe Vieira Frujeri, Chaim Hoch, Srikanth Kandula, Ishai Menache, Michael Schapira, and Aviv Tamar. 2023. {DOTE}: Rethinking (Predictive){WAN} Traffic Engineering. In *20th USENIX Symposium on Networked Systems Design and Implementation (NSDI 23)*. 1557–1581.
- [37] Leon Poutievski, Omid Mashayekhi, Joon Ong, Arjun Singh, Mukarram Tariq, Rui Wang, Jianan Zhang, Virginia Beauregard, Patrick Conner, Steve Gribble, et al. 2022. Jupiter evolving: transforming google’s datacenter network via optical circuit switches and software-defined networking. In *Proceedings of the ACM SIGCOMM 2022 Conference*. 66–85.
- [38] Harald Racke. 2002. Minimizing congestion in general networks. In *The 43rd Annual IEEE Symposium on Foundations of Computer Science, 2002. Proceedings.* IEEE, 43–52.
- [39] Matthew Roughan, Albert Greenberg, Charles Kalmanek, Michael Rumsewicz, Jennifer Yates, and Yin Zhang. 2002. Experience in measuring backbone traffic variability: Models, metrics, measurements and meaning. In *Proceedings of the 2nd ACM SIGCOMM Workshop on Internet Measurement*. 91–92.
- [40] Matthew Roughan, Mikkel Thorup, and Yin Zhang. 2003. Traffic engineering with estimated traffic matrices. In *Proceedings of the 3rd ACM SIGCOMM Conference on Internet Measurement*. 248–258.
- [41] Arjun Roy, Hongyi Zeng, Jasmeet Bagga, George Porter, and Alex C Snoeren. 2015. Inside the social network’s (datacenter) network. In *Proceedings of the 2015 ACM Conference on Special Interest Group on Data Communication*. 123–137.
- [42] Ankit Singla, Chi-Yao Hong, Lucian Popa, and P Brighten Godfrey. 2012. Jellyfish: Networking data centers randomly. In *9th USENIX Symposium on Networked Systems Design and Implementation (NSDI 12)*. 225–238.
- [43] Martin Suchara, Dahai Xu, Robert Doverspike, David Johnson, and Jennifer Rexford. 2011. Network architecture for joint failure recovery and traffic engineering. *ACM SIGMETRICS Performance Evaluation Review* 39, 1 (2011), 97–108.
- [44] Min Yee Teh, Shizhen Zhao, Peirui Cao, and Keren Bergman. 2020. COUDER: robust topology engineering for optical circuit switched data center networks. *arXiv preprint arXiv:2010.00090* (2020).
- [45] Min Yee Teh, Shizhen Zhao, Peirui Cao, and Keren Bergman. 2022. Enabling quasi-static reconfigurable networks with robust topology engineering. *IEEE/ACM*

- Transactions on Networking* (2022).
- [46] Renata Teixeira, Sharad Agarwal, and Jennifer Rexford. 2005. BGP routing changes: Merging views from two ISPs. *ACM SIGCOMM Computer Communication Review* 35, 5 (2005), 79–82.
 - [47] Steve Uhlig, Bruno Quoitin, Jean Lepropre, and Simon Balon. 2006. Providing public intradomain traffic matrices to the research community. *ACM SIGCOMM Computer Communication Review* 36, 1 (2006), 83–86.
 - [48] Asaf Valadarsky, Michael Schapira, Dafna Shahaf, and Aviv Tamar. 2017. Learning to route. In *Proceedings of the 16th ACM workshop on hot topics in networks*. 185–191.
 - [49] Hao Wang, Haiyong Xie, Lili Qiu, Yang Richard Yang, Yin Zhang, and Albert Greenberg. 2006. COPE: Traffic engineering in dynamic networks. In *Proceedings of the 2006 conference on Applications, technologies, architectures, and protocols for computer communications*. 99–110.
 - [50] Yue Wang, Yongbin Sun, Ziwei Liu, Sanjay E Sarma, Michael M Bronstein, and Justin M Solomon. 2019. Dynamic graph cnn for learning on point clouds. *ACM Transactions on Graphics (tog)* 38, 5 (2019), 1–12.
 - [51] Kuai Xu, Zhi-Li Zhang, and Supratik Bhattacharyya. 2005. Profiling internet backbone traffic: behavior models and applications. *ACM SIGCOMM Computer Communication Review* 35, 4 (2005), 169–180.
 - [52] Zhiying Xu, Francis Y Yan, Rachee Singh, Justin T Chiu, Alexander M Rush, and Minlan Yu. 2023. Teal: Learning-Accelerated Optimization of WAN Traffic Engineering. In *Proceedings of the ACM SIGCOMM 2023 Conference*. 378–393.
 - [53] Rex Ying, Ruining He, Kaifeng Chen, Pong Eksombatchai, William L Hamilton, and Jure Leskovec. 2018. Graph convolutional neural networks for web-scale recommender systems. In *Proceedings of the 24th ACM SIGKDD international conference on knowledge discovery & data mining*. 974–983.
 - [54] Nicu Florin Zaicu, Matthew Luckie, Richard Nelson, and Marinho Barcellos. 2021. Helix: Traffic Engineering for Multi-Controller SDN. In *Proceedings of the ACM SIGCOMM Symposium on SDN Research (SOSR)*. 80–87.
 - [55] Hengrui Zhang, Zhongming Yu, Guohao Dai, Guyue Huang, Yufei Ding, Yuan Xie, and Yu Wang. 2022. Understanding gnn computational graph: A coordinated computation, io, and memory perspective. *Proceedings of Machine Learning and Systems* 4 (2022), 467–484.
 - [56] Zhizhen Zhong, Manya Ghobadi, Alaa Khaddaj, Jonathan Leach, Yiting Xia, and Ying Zhang. 2021. ARROW: restoration-aware traffic engineering. In *Proceedings of the 2021 ACM SIGCOMM 2021 Conference*. 560–579.

APPENDIX

Appendices are supporting material that has not been peer-reviewed.

A NOTATION TABLE

In this section, we tabulate the notations in Table 6.

Notation	Description
$G(V, E, c)$	Network topology, V is vertex set, E is edge set, and c assigns capacities to edges
D	Demand matrix, where D_{ij} denotes the traffic from i to j
P	Network paths, where P_{sd} denotes the set of network paths through which source s communicates with destination d
C_p	The capacity of path p
r_p	The split ratio of the traffic demand from s to d forwarded along path p
\mathcal{R}	TE configuration
$M(\mathcal{R}, D)$	MLU in the network given D and \mathcal{R}
Δ	The set representing mismatch
\mathcal{S}_p	Path sensitivity for path p
\mathcal{S}_{sd}^{\max}	Maximum path sensitivity among all paths in P_{st}
\mathcal{F}	Function for path sensitivity constraints
π_θ	The mapping function from DNN inputs to outputs, and θ denotes the DNN's weight
H	Window length, representing the number of historical traffic demands in the DNN input
$\mathcal{L}(\mathcal{R}_t, D_t)$	Loss function
$\sigma_{D_{sd}, [1-T]}^2$	The variance of traffic demands D_{sd} within the time range from 1 to T

Table 6: Notations used in this paper

B TE OPTIMIZATION FORMULATION

In this section, we formulate the TE optimization problem. Given a network $G(V, E, c)$ and traffic demand D , to find an optimal TE configuration which specifies a split ratio r_p for each path $p \in P_{st}$, where r_p represents the fraction of the traffic demand from s to t forwarder along path p , the optimization formulation shown in Equation 9 can be established.

$$\begin{aligned}
 & \underset{\mathcal{R}}{\text{minimize}} && \max_{e \in E} \frac{f_e}{c(e)} \\
 & \text{subject to} && \sum_{p \in P_{st}} r_p = 1, \forall s, t \in V \\
 & && \sum_{s, t \in V, p \in P_{st}, e \in p} D_{st} \times r_p = f_e, \forall e \in E
 \end{aligned} \tag{9}$$

Our work, however, focuses on realistic scenarios where TE schemes must select configurations on the realistic scenario in which the traffic demand is not known beforehand.

C HEURISTIC SELECTION OF \mathcal{F}

In this section, we integrate the Desensitization-based TE scheme in Google's Jupiter Evolving [37], replacing its fixed path sensitivity constraints with a heuristically selected function $\mathcal{F} : (s, t) \rightarrow \mathbb{R}^+$. As discussed in §4, for stable traffic, we apply lenient sensitivity constraints, whereas, for highly bursty traffic, we impose stringent constraints. We use traffic variance as an indicator of traffic burstiness. Therefore, the path sensitivity constraints should become increasingly stringent as the path variance increases, meaning the maximum allowable path sensitivity should decrease correspondingly. We experiment with two heuristic functions: 1) Linear function, and 2) Piecewise function.

C.1 Linear function

The function we have selected is illustrated in Figure 9. Using a linear function, we arrange the traffic variance for all SD pairs in ascending order and assign varying path sensitivity constraints based on different orders. The *Max* and *Min* values in the Figure can be arbitrarily chosen, but ensuring that a solution is feasible when selecting *Min* is crucial. For instance, if there are n paths serving this SD pair, each with capacity of 1, it is required that $r_p \leq \text{Min}$ and $\sum_{i=1}^n r_i = 1$. In this scenario, *Min* should not be less than $\frac{1}{n}$; otherwise, the problem becomes unsolvable.

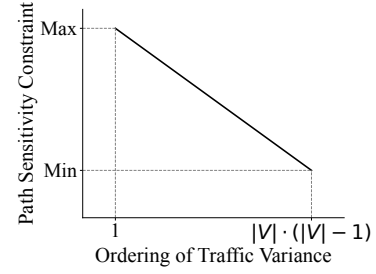


Figure 9: Illustrating the function \mathcal{F} selected by Linear function.

We conduct tests using varying *Min* and *Max* parameters, which are listed in Table 7. Strategy 1 refers to the implementation of stricter path sensitivity restrictions. In contrast, Strategy 2 involves relaxing the path sensitivity restrictions for more stable flows. Meanwhile, Strategy 3 suggests a combination approach: it proposes enforcing stricter path sensitivity restrictions on sudden or bursty flows while simultaneously relaxing these restrictions for stable flows. For ease of numerical representation, we have normalized the capacities of all paths in the graph, setting the smallest capacity to 1, with other capacities calculated proportionally.

We apply the parameters listed in Table 7 and conduct tests on the PoD-level Meta DB. The results are summarized in Figure 10. As shown in Figure 10, the application of Strategy 1, which involves imposing stricter path sensitivity constraints (as in the case of the group {1,2,3}), leads to an enhanced capability to handle bursty traffic. On the other hand, with the implementation of Strategy 2, an improvement in average performance is observed, as demonstrated by the comparison of groups {3,4}. Comparing

	Strategy 1		Original	Strategy 2	Both
Number	1	2	3	4	5
Min	1/3↓	1/3↓	2/3	2/3	1/3↓
Max	1/2↓	2/3	2/3	5/6↑	5/6↑

Table 7: The parameters selected for the Linear function. ‘Original’ refers to the fixed path sensitivity constraint of the Desensitization-based TE.

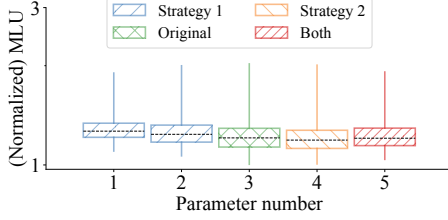


Figure 10: Comparing the TE quality under different parameter settings in Linear function. The parameter number on the x-axis corresponds to the numbering in Table 7

parameters 5 with parameters 1, we observe that by maintaining the sensitivity constraint for high bursty traffic while relaxing the sensitivity constraint for non-bursty traffic, parameters 5 can reduce the normal-case performance (below the 75th percentile) MLU by 5% at the expense of increasing the peak MLU by 0.7%.

C.2 Piecewise function

The function we have selected for our analysis is depicted in Figure 11. It utilizes a piecewise approach to define constraints on path sensitivity, following the same x-axis and y-axis interpretations as shown in Figure 9. We specifically chose a piecewise function for this purpose. We introduce a breakpoint within the function to distinguish between stable and bursty traffic conditions. For traffic variances that fall below this breakpoint, indicative of stable flow, the path sensitivity constraints are comparatively relaxed. In contrast, for traffic variances that exceed this breakpoint, representing bursty flow, the constraints are tighter and more rigorous.

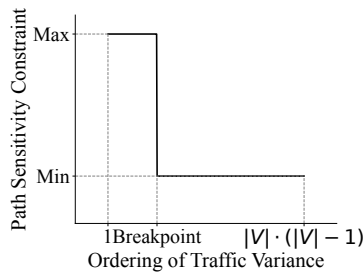


Figure 11: Illustrating the function \mathcal{F} selected by Piecewise function.

We employ various parameters to demonstrate the impact of different parameter settings on the results. In this function, the parameters available for selection include *Min*, *Max*, and *breakpoint*. Our parameter settings are presented in Table 8. For ease of numerical representation, we have normalized the capacities of all paths in the graph, setting the smallest capacity to 1, with other capacities calculated proportionally. Additionally, we represent the value of the breakpoint in terms of its proportion rather than as an absolute number. For example, breakpoint=0.8 signifies that the first 80% of the flow is relatively stable, while the latter 20% comprises bursty traffic.

	Strict Constraint			Original	Relaxed Constraint		
Number	1	2	3	4	5	6	7
Min	1/2↓	1/2↓	1/2↓	2/3	2/3	2/3	2/3
Max	2/3	2/3	2/3	2/3	5/6↑	5/6↑	5/6↑
Breakpoint	0.5	0.65	0.8	\	0.5	0.65	0.8

Table 8: The parameters selected for the Piecewise function. ‘Original’ refers to the fixed path sensitivity constraint of the Desensitization-based TE.

In our study, we conducted a series of tests on the parameters listed in Table 8 on PoD-level Meta DB, with the results summarized in Figure 12. As illustrated in the figure, with fixed values of *Min* and *Max*, a larger Breakpoint setting enhances the average performance of TE methods. This trend is evident in groups {1,2,3} and {5,6,7}, where an increase in Breakpoint corresponds to a lower average performance boxplot. Conversely, with a constant Breakpoint, maintaining *Max* while reducing *Min* enhances the TE methods’ ability to manage bursty traffic, as shown in the comparison of group {1,4}. Similarly, fixing *Min* while increasing *Max* leads to better average performance of TE methods, as observed in the comparison between groups {4,5}.

These findings align with intuitive expectations: a higher proportion of stable traffic or more lenient path sensitivity constraints for stable traffic result in improved average algorithm performance. Conversely, a lower proportion of stable traffic with stricter constraints for bursty traffic enhances the algorithm’s ability to handle sudden bursts.

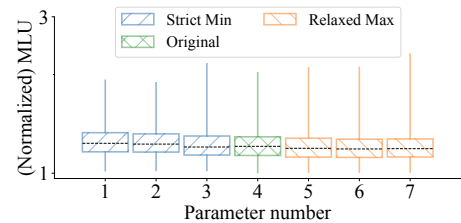


Figure 12: Comparing the TE quality under different parameter settings in Piecewise function. The parameter number on the x-axis corresponds to the numbering in Table 8.

C.3 Summary

This section demonstrates that by implementing fine-grained robustness enhancement strategies into Google's TE using simple heuristic functions, we can achieve varying effects through parameter adjustments, thereby enhancing the original TE algorithm's capabilities. Our application of deep learning in FIGRET aims to identify the function form and parameters for fine-grained robustness enhancement as effectively as possible, while also speeding up the TE solution process.

D FIGRET IMPLEMENTATION DETAILS

While we have chosen FCN among FCN, CNN, and GNN for our application, this does not imply that TE problems must exclusively use FCNs. More sophisticated and advanced network architectures can be further explored.

D.1 No need for GNN

The mapping between TE configuration and Maximum Link Utilization (MLU) can be represented using Function 1. As seen from Function 1, this mapping can be established through simple matrix operations.

Function 1: Mapping traffic configurations to MLU

- 1 $G = (V, E, c)$ // Graph that models the network topology
 - 2 $\Omega = \{(i, j) | i \in V, j \in V, i \neq j\}$ // the set of all source-destination (SD) pairs
 - 3 $\Phi = \bigcup_{s, t \in \Omega} P_{st}$ // the set of all paths
 - 4 $SDtoPath^{|\Omega| \times |\Phi|}$ // Signifies whether path j serves the SD pair i . $SDtoPath_{i,j} = 1$ if path j serves SD pair i , 0 otherwise
 - 5 $PathtoEdge^{|\Phi| \times |E|}$ // Signifies whether path i contains edge j . $PathtoEdge_{i,j} = 1$ if edge $j \in$ path i , 0 otherwise
 - 6 $\mathcal{R}^{|\Phi| \times 1}$ // Network configuration yields the split ratios for all paths
 - 7 $C^{|E| \times 1}$ // vector representing link capacities
 - 8 $DM_{|\Omega| \times 1}$ // Flatten traffic demand matrix
/* Compute MLU form $\mathcal{R} \times$ for matrix multiplication; \odot for element-wise (Hadamard) multiplication */
 - 9 $FlowOnPath^{|\Phi| \times 1} = SDtoPath^T \times DM \odot \mathcal{R}$
// $(|\Phi|, |\Omega|) \times (|\Omega|, 1) \odot (|\Phi|, 1)$, calculate the flow on each path
 - 10 $FlowOnEdge^{|E| \times 1} = PathtoEdge^T \times FlowOnPath$
// $(|E|, |\Phi|) \times (|\Phi|, 1)$, calculate the flow on each edge
 - 11 $MLU = \text{Max}(FlowOnEdge/C)$
-

D.2 The inappropriateness of CNN

In Figure 13, there is a source s and three destinations t_1, t_2, t_3 , with a convolution kernel size of 2. This kernel aims to extract local information of length 2 from the traffic demands. However, extracting local information between d_1, d_2 and d_2, d_3 proves ineffective because p_{st_1} and p_{st_2} , as well as p_{st_2} and p_{st_3} , do not share a common

edge. Conversely, p_{st_1} and p_{st_3} do share a common edge, and their traffic demands should be considered jointly. This limitation cannot be addressed by such convolution layers that are designed to extract local information. Unlike image data, which CNNs excel at handling due to the localized relevance of information, TE problems do not exhibit a distinct need for extracting local information because traffic demands within a convolutional locality may not necessarily pass through a common edge, making the use of convolution for local information extraction minimally effective. Therefore, in our model design, we chose not to incorporate convolutional layers. Instead, we opted for directly utilizing fully connected layers.

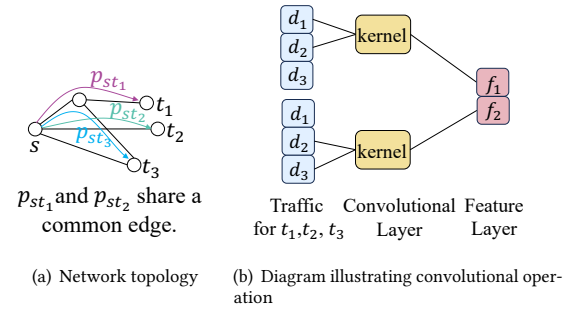


Figure 13: Diagram illustrating the convolution operation in TE. Traffic demands for paths that share a common edge need to be considered jointly due to their potential impact on each other. In contrast, for paths without a shared edge, jointly considering their traffic demands is ineffective.

D.3 Drawbacks of Using RL

Reinforcement learning is extensively applied in Traffic Engineering (TE), as exemplified by TEAL [52]. This method learns strategies for achieving objectives in complex environments through trial and error. However, it often comes with high computational complexity and sensitivity to parameter settings. In TE, the relationship between policies—TE configurations and the objective of minimizing link utilization (MLU) is quite explicit and can be directly expressed. In such relatively simple scenarios, reinforcement learning may not be the most optimal choice. Under these circumstances, it's unnecessary to undergo the complex exploration and trial-and-error adjustments typical of reinforcement learning. Instead, direct application of gradient descent methods could be more effective.

In Table 2, we present a comparison of the training times for FIGRET and TEAL, which involve GNN and reinforcement learning, as well as the precomputation time for Oblivious and COPE. It is evident that as the network topology scales up, FIGRET's precomputation time offers a greater advantage.

D.4 Implementing FIGRET

DNN architecture. Similar to DOTE, except for the input and output layers, FIGRET uses five fully connected neural network layers with 128 neurons each and employs ReLU(x) activation, except for the output layer, which uses Sigmoid(x).

Optimizer. During the training process, FIGRET employs the Adam optimizer [28] for stochastic gradient descent.

E ADDITIONAL LINK FAILURE RESULTS

In this section, we present the results from evaluating link failures on pFabric and ToR-level DC Meta DB, as shown in Figures 14 and 15. As can be seen in Figure 15, when the network traffic demands exhibit high dynamics, the current TE scheme in Google's Jupiter data centers, even with the knowledge of which links are going to fail, fails to achieve satisfactory results.

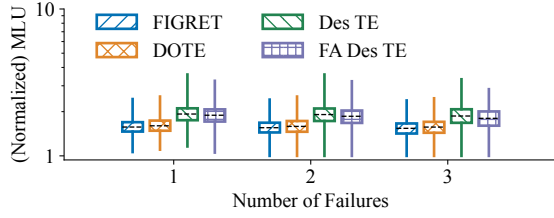


Figure 14: Coping with different numbers of random link failures on pFabric.

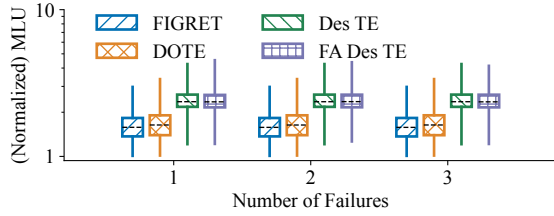


Figure 15: Coping with different numbers of random link failures on ToR-level Meta DB.

F VISUALIZATION OF TRAFFIC DEMANDS

To visually demonstrate the extent of traffic data migration over time, we conduct a visualization analysis of traffic demands from both the PoD-level Meta DB and the ToR-level Meta DB using the t-distributed stochastic neighbor embedding (t-SNE) method [22] in this section. We analyze their traffic from 0% to 100% using t-SNE and compare the differences in the intervals of 0% – 25%, 25% – 50%, 50% – 75%, and 75% – 100%. The 2-dimensional t-SNE components are plotted in Figure 16 and Figure 17.

From the results, we observe the following:

- Compared to the PoD-level data, the ToR-level data is more dispersed, indicating a higher dynamism in ToR-level traffic data.
- Both ToR-level and PoD-level data exhibit a single cluster formation in the t-SNE plots, suggesting their traffic patterns do not undergo drastic changes over time.
- While the PoD-level data remains very similar across all four-time segments, the ToR-level data shows some variations.

These observations are consistent with our evaluation results, indicating firstly that TE is more challenging at the ToR-level (§5.2) and, secondly, that FIGRET's robustness to time drift performs well at both levels (§5.4). Moreover, the impact of time drift on FIGRET's effectiveness is greater at the ToR-level (§5.4).

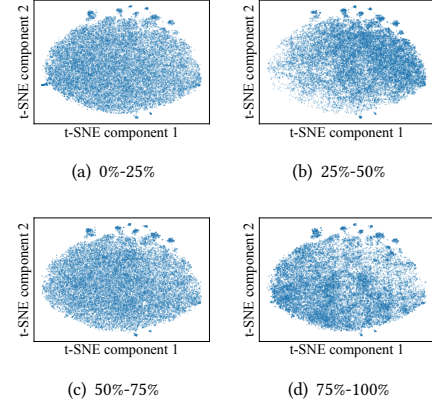


Figure 16: Visualizing Traffic Demands of the PoD-level Meta DB using the t-SNE Method.

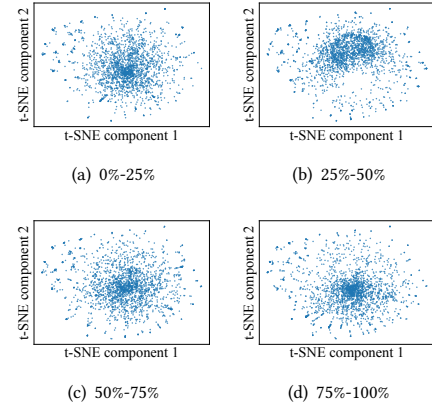


Figure 17: Visualizing Traffic Demands of the ToR-level Meta DB using the t-SNE Method.

G A CLOSER LOOK AT THE DRAWBACKS OF EXISTING TE SCHEMES

G.1 Objective mismatch in Demand-prediction-based TE

In demand-prediction-based TE, a notable mismatch exists between the objective of accurately predicting future traffic and minimizing the MLU [36]. This mismatch primarily arises from the influence of network topology on MLU, indicating that traffic demands exert varied impacts on MLU. For instance, traffic traversing paths with higher capacity tends to have a lesser effect on MLU. Similarly,

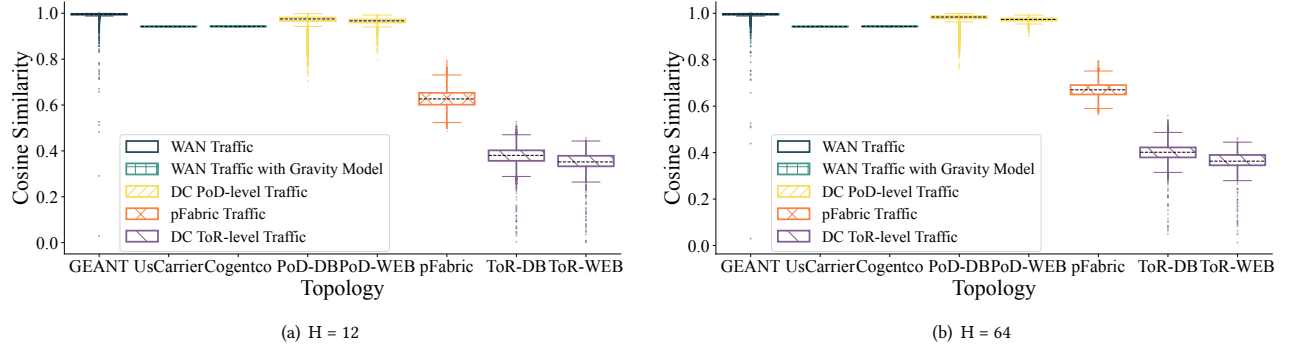
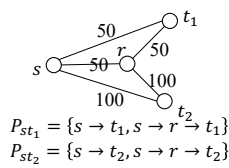


Figure 18: Cosine similarity analysis using a window of H historical TMs vs. the currently-seen TM.

traffic flowing through paths without shared edges with other paths will also impact MLU to a lesser degree. An example illustrating this concept is provided in Figure 19.



(a) In the network topology, where numbers on edges indicate link capacity, traffic demands of d_1 and d_2 need to be sent from s to t_1 and s to t_2 , respectively.

Predicted (d_1, d_2)	Split ratio ($\eta_{\{s \rightarrow t_1\}}, \eta_{\{s \rightarrow t_2\}}$)	MLU
(50, 60)	(11/20, 11/12)	0.66
(60, 50)	(1/2, 1)	0.6
Upcoming Demand: (60, 60)		

(b) An example concerning predicted traffic, where the split ratios are only specified for the paths $s \rightarrow t_1$ and $s \rightarrow t_2$, with the split ratios for the other two paths being 1 minus the corresponding split ratios.

Figure 19: An example demonstrating the mismatch between achieving accurate traffic predictions and minimizing MLU. Two predicted demands achieve the same level of prediction accuracy (with identical mean-square-error values). However, the optimal split ratios derived from these two traffic predictions lead to different MLUs. Incorrect predictions of the traffic from s to t_2 have a lesser impact on MLU. This is due to the larger capacity of the path from s to t_2 .

G.2 Limited gains from window expansion

Deep learning approaches demonstrate powerful capabilities in using information within a window to obtain a better D^{expect} . Therefore, in this section, we consider whether, under the premise of sufficient computational power and memory, expanding the window size could make D^{expect} highly accurate and prevent mispredictions, thereby eliminating the need to consider sudden traffic changes. Using an analysis method similar to §5, we examine the cosine similarity between upcoming traffic and traffic from the past H time windows, where H is increased to 64. The results are summarized in Figure 18. However, the results indicate that, regardless of whether in stable or bursty network types, the cosine similarity does not significantly increase compared to when H is 12,

suggesting that expanding the window size is *ineffective* in avoiding sudden traffic changes.

Due to the limited information within the window, DOTE, which solely relies on window-based information and prioritizes MLU, may result in suboptimal configurations. An example is shown in Figure 20, which illustrates an inadequate network configuration by DOTE on the ToR-level Meta DB (with an Omniscient-normalized MLU of 2.86). We selected the SD pair responsible for the MLU, and as seen in Figure 20(a), the traffic on this SD pair was consistently stable at a relatively low value. Therefore, DOTE assigned a configuration for this SD pair involving paths with high path sensitivity. However, in the next time snapshot, the SD pair burst unexpectedly, significantly impacting the highly sensitive paths, leading to high MLU.

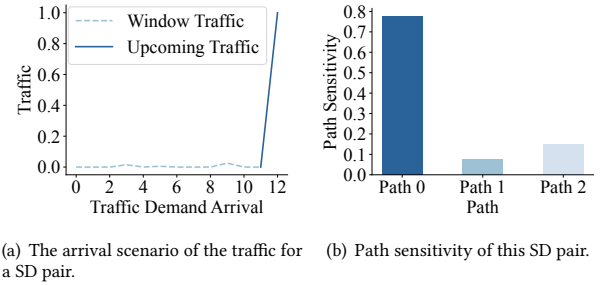


Figure 20: Showcasing the limitations of the DOTE approach.